Simulation of a Rapid Compression Machine for Evaluation of Ignition Chemistry and Soot Formation Using Gasoline/Ethanol Blends

Musharrat Chowdhury
Marquette University

SIMULATION OF A RAPID COMPRESSION MACHINE FOR EVALUATION OF IGNITION CHEMISTRY AND SOOT FORMATION USING GASOLINE/ETHANOL BLENDS

by

Musharrat Chowdhury

A Thesis submitted to the Faculty of the Graduate School,
Marquette University,
in Partial Fulfillment of the Requirements for
the Degree of Master of Science

Milwaukee, Wisconsin

December 2022

ABSTRACT
SIMULATION OF A RAPID COMPRESSION MACHINE FOR EVALUATION OF IGNITION CHEMISTRY AND SOOT FORMATION USING GASOLINE/ETHANOL BLENDS

Musharrat Chowdhury

Marquette University, 2022

With the projected decline of demand for gasoline in light duty engines and the advent of ethanol as a green fuel, the use of gasoline-ethanol blend fuels in heavy duty applications are being investigated where the primary mode of combustion is mixing controlled combustion. In mixing controlled combustion, a wide range of mixture conditions (equivalence ratio) exist inside the engine cylinder. The sooting tendencies of light fuels at richer conditions are not well understood. The goal of this research is to model the particulate matter emissions for gasoline/ethanol fuel blends, especially at fuel rich conditions. The computational models can then be used with in-cylinder conditions to predict the emissions characteristics of light fuel blends.

The ethanol-gasoline blend fuels are modelled in a three-dimensional numerical simulation in a Rapid Compression Machine (RCM) using CONVERGE computational software. Several chemical kinetic mechanisms are used with SAGE chemistry solver and a RANS k-e turbulence model with a geometrically accurate sector model of the RCM including the creviced piston. The creviced piston is used in the experimental setup to reduce boundary layer effects and to maintain a homogeneous core in the reaction cylinder. The reaction mechanisms have been previously validated at engine like conditions for different fuel blends. Computational fluid dynamics simulations are conducted for different gasoline-ethanol fuel blends from E10 (10% ethanol v/v) to E100. The fuel blend is modelled as a surrogate mixture of toluene, di-iso-butane, iso-octane, n-heptane for gasoline content, and ethanol. The computational results were validated against experimental results from an optical RCM using pressure measurements and laser extinction diagnostics. Different soot models and kinetic mechanisms are investigated to accurately predict the sooting tendencies of fuel blends, especially in richer conditions experienced during mixing-controlled combustion.

The experimental combustion characteristics of different blends of fuel as well as soot generation are reasonably well predicted indicating that the use of the computational model can be extended to predict particulate matter emissions in heavy duty engine conditions.

ACKNOWLEDGMENTS

Musharrat Chowdhury

Firstly, I would like to thank my advisor Dr. Adam B. Dempsey for his sage guidance throughout this research project. His knowledge and passion for research, and his wide network within the engine research community has helped make progress at every step. Thanks to Dr. Casey M. Allen, for his wisdom and direction in exploring the world of RCMs. I would also like to thank all of my colleagues in the Marquette University Engine Research Lab for their help and contribution throughout my graduate studies.

Secondly, I would like to thank Convergent Science, which provided CONVERGE licenses and technical support for this work. I would especially like to acknowledge Dr. Sameera Wijeyakulasuriya, who has helped resolve numerous obstacles and answer many questions in my quest of this project.

I would also like to thank my family for their continuous encouragement. With your loving support I will always strive to reach the sky. Special gratitude to my partner, Paean, for her endless love and support through all my worldly adventures.

Lastly, I would like to extend my gratitude to the Opus College of Engineering and Graduate School of Marquette University as well as the faculty and staff for nurturing an environment encouraging academic excellence and advanced research. Special thanks to the Marquette University HPC team for maintaining the cluster, RAJ, which has enabled this work.

TABLE OF CONTENTS

LIST OF TABLES

LIST OF FIGURES

CHAPTER 1

INTRODUCTION

1.1 Background and Motivation

The internal combustion engine (ICE) has been an integral part of human development for over a 150 years with wide applications in personal and commercial transportation on land, air and sea, energy production, agriculture, construction and various other fields. The traditional fossil fuels used in IC engines, like diesel and gasoline, form many harmful pollutants such as Nitrogen Oxides (NOx), unburned hydrocarbons (UHC), carbon monoxide (CO), carbon dioxide (CO2) and particulate matter (PM). According to the Intergovernmental Panel on Climate Change (IPCC) and the United States Environmental Protection Agency (EPA), carbon dioxide alone accounts for nearly 80% of the global greenhouse gas emissions. Use of fossil fuels and industrial processes make up around 85% of the total carbon dioxide emissions [34,75]. Nitrous Oxides account for another 6% of greenhouse gas emissions.

All of these pollutants have major effects on local and global climate as well as human health. In face of these issues and in the pursuit of higher efficiency and lower emissions, there has been a continuous push to find solutions with lesser environmental effects. According to the predictions of the US EPA as illustrated in Figure 1.1, the energy consumption in transportation sector will see growth; the majority demand met by liquid fuels. They are also predicting a massive rise of biofuel production (Figure 1.1b). The major question is, how can we use this growth in biofuel production to build sustainalbe transportation solutions?

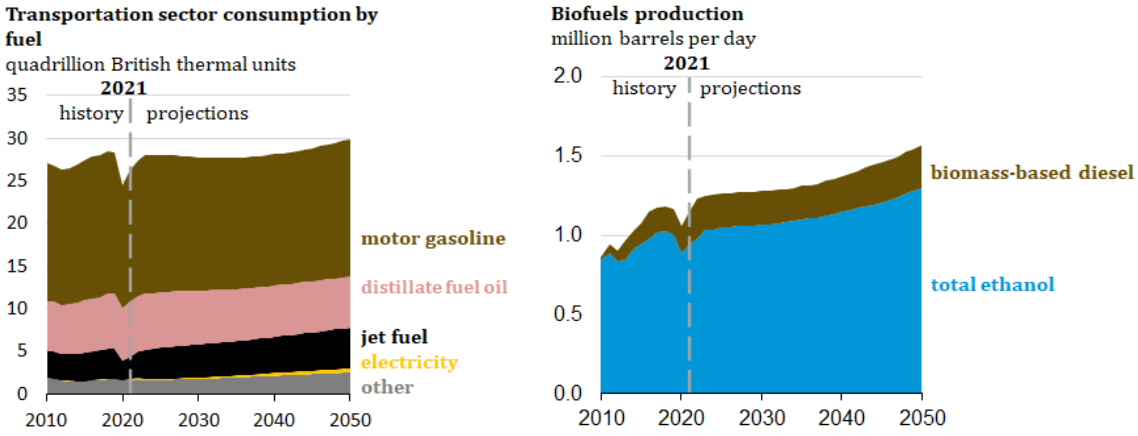

(a) Main Chamber Pressure Traces (b) Cumulative Heat Release Rates

Figure 1.1: Energy Outlook Predictions

1.2 Advanced Combustion Strategies

In response to climate change as well as depleting petroleum resources, focus has shifted to finding alternative solutions, such as renewable energy sources, electrification of the transportation sector etc. There has also been an increased focus from combustion researchers and manufacturers on developing advanced combustion strategies improving upon the existing IC engine platform offering reduced emissions and higher efficiency. Many of these strategies also aim at using alternative renewable fuels which help closing the carbon life cycle and reduce the CO_2 emissions [48].

These advanced combustion strategies often use some variation of compression ignition due to advantages associated with globally lean operations. One such strategy that has been studied extensively is the Homogeneous charge compression ignition (HCCI) [61]. This strategy combines the advantages of both spark ignition and compression ignition combustion strategies resulting in near zero particulate matter and NOx emissions as well as higher thermodynamic efficiency, lower heat transfer losses and fast combustion [82]. Despite these

benefits HCCI lacks control over combustion phasing [6] which has lead research into alternative concepts of combustion. Research has been made into combustion phasing control through use of valve timing, intake temperature control, exhaust gas recirculation [4,5,18,35,73,83]; however these methods have their own challenges regarding maintaining stable combustion phasing and operational window.

Investigation has also been done to achieve combustion phasing control over a wide range of operation conditions through in-cylinder reactivity stratification; either by fuel reactivity stratification [11,13,17,18,20,33,42–44,49] or thermal stratification [14,15,22,23,47,64,69,70]. Other methods previously and currently being research is using ignition assistant devices like glowplugs [58,85], pre-chambers [16] or even spark plugs [9,67] to initiate combustion in a compression ignition like manner. One thing that many of these combustion strategies have in common is the the existence of a wide range of equivalence ratio in cylinder and the use of lighter fuels such as gasoline, ethanol, methanol or a blend of these fuels. The particulate matter emissions characteristics of these light fuels are still not well understood at the richer conditions seen within a mixing controlled combustion event. Research has been done in an attempt to understand the sooting tendencies of pure gasoline or ethanol fuels as well as their blends [10,37,38,81] in various engine like condition but there is still a lot of work to be done in modeling soot emissions of these light blend fuels at rich conditions and at different blend levels.

1.3 Research Objective

One strategy to reduce the environmental impact of heavy duty engines is the increasing use of greener fuels such as alcohols (ethanol, methanol) or a blend of these fuels with gasoline or diesel. The primary mode of combustion for heavy

duty engines is mixing controlled combustion due to advantages with load management, efficiency, robustness of combustion etc. In a mixing controlled combustion environment a wide range of equivalence ratio exists. These lighter fuels have higher octane number i.e. lower reactivity so they are not well suited for direct adaptation into compression ignition engines. There needs to be some kind of ignition assistance, especially at unfriendly conditions. One method to achieve this is using a prechamber in conjunction with a direct injector to burn ethanol. With direct injections one of the biggest concerns are sooting tendencies at higher equivalence ratios since the fuel injection is stratified.

This study aims to understand how these fuels behave under fuel rich conditions. The two pronged approach sees experiments with an optical Rapid Compression Machine (RCM) and a numerical simulation model for fundamental understanding of soot formation process for these fuels. A rapid compression machine provides a highly repeatable experimental process isolating the fuel chemical kinetics from the inherent complexities associated with engines such as effects turbulence chemistry interactions, cycle to cycle variability, engine breathing etc. [72]. The homogeneous mixture also removes variables associated with spray modeling e.g., fuel evaporation, atomization, air entrapment etc. These qualities make the RCM an ideal candidate for building a CFD model using appropriate chemical kinetics mechanisms and soot models that can accurately capture the sooting tendencies of gasoline-ethanol blend fuels at different conditions starting from fairly low temperature/pressure conditions in the RCM to heavy duty engine like conditions.

CHAPTER 2

RCM: EXPERIMENTAL SETUP

2.1 Overview

This chapter will discuss the experimental equipment and facilities used for the study of the soot formation characteristics of gasoline-ethanol blend fuels. An optical Rapid Compression Machine (RCM) was used to study the chemical kinetics and soot formation behaviour of different blends of gasoline ethanol fuels from E10 to E100. Figure 2.1 illustrates the Rapid Compression Machine used in this study.

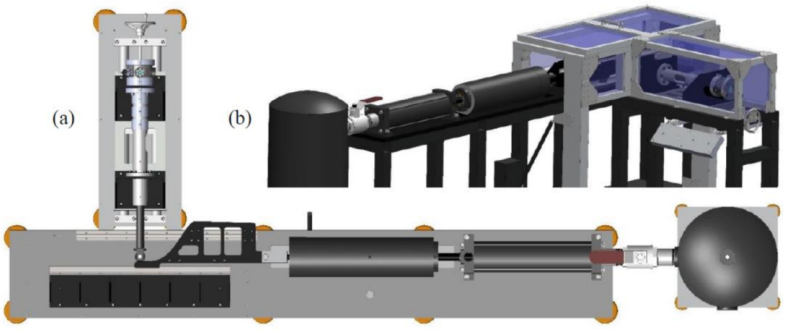

Figure 2.1: RCM design (a) Top View (b) Isometric View [39]

2.2 Design of the RCM

The RCM used in the experiments is pneumatically driven via a cam with constant profile to drive the piston. After reaching the top dead center (TDC), a hydraulic braking piston holds the test piston cylinder assembly in a constant volume. This process results in a fast compression of charge to a suitable auto-ignition condition. Table 2.1 gives an overview of some of the physical design characteristics of the RCM.

Table 2.1: RCM Design Characteristics

Cylinder Bore	2 in
Stroke Length	8 in
Compression Ratio	4-19
Compression Time	∼30-50 ms

The cam used for the RCM has a constant stroke length of 8″. The compression ratio can be varied through the movement of the test cylinder. This provides a fine control over the compression ratio and provides a wide range of testing conditions. Figure 2.2 shows a dimensional drawing of the RCM highlighting the stroke and compression profile.

The piston of the RCM is an optimized creviced design [57]. This creviced piston design helps maintain a homogeneous core after full compression by scooping up the boundary layer during compression. This ensures that the compressed charge is at a homogeneous temperature and pressure instead of the thin boundary layer around the cylinder being at colder temperatures.

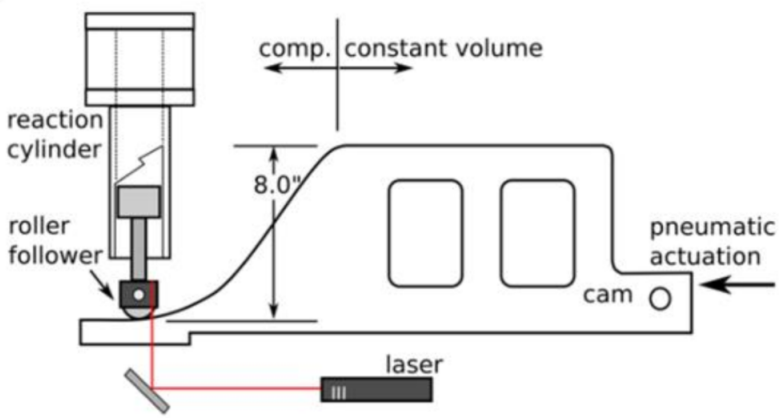

Figure 2.2: Dimensional illustration of the RCM highlighting the stroke and compression profile

2.3 Instrumentation and Control

In cylinder pressure data is recorded through a Kistler 6045A piezoelectric pressure transducer installed in the head of the RCM. The pressure transducer samples at a rate of 100 kHz.

The RCM is fully heated at a steady temperature through a series of heating bands and thermocouples operating under a PID controller. A custom insulation blanket provides insulation and ensures thermal equilibrium throughout the test domain. This well designed heating system ensures that any gas inside the RCM reaches a thermal equilibrium. The initial temperature of the RCM can be varied from 40 °C to 120 °C.

2.4 Optical Diagnostics

Soot formation inside the RCM is quantified with a liner-of-sight laser extinction diagnostic setup. In this setup, the laser passes through the cylinder via two fused silica windows at opposite sides at of the cylinder. The windows are located near the cylinder head to ensure the higher compression ratios would not obstruct the view. The laser used for the setup is a 22.5 mW He-Ne laser (λ = 632.8 mm). Figure 2.3 shows the path of the laser through the RCM.

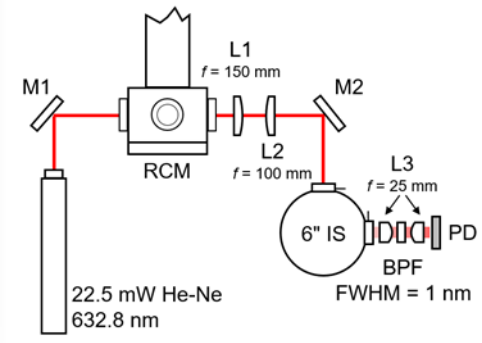

Figure 2.3: Laser extinction diagnostic setup

As the laser passes through the cylinder, it is attenuated due to absorption and scattering by the soot particles, this results in a reduction of the incident intensity which is captured by the photodetector. One concern due to the high temperature and density gradients created in the cylinder is beam steering. Beam steering refers to bending of the laser from the changes in the refractive index of the gas due to high temperature and density gradients. The optics were optimized to ensure that the beam steering did not affect the soot formation measurements.

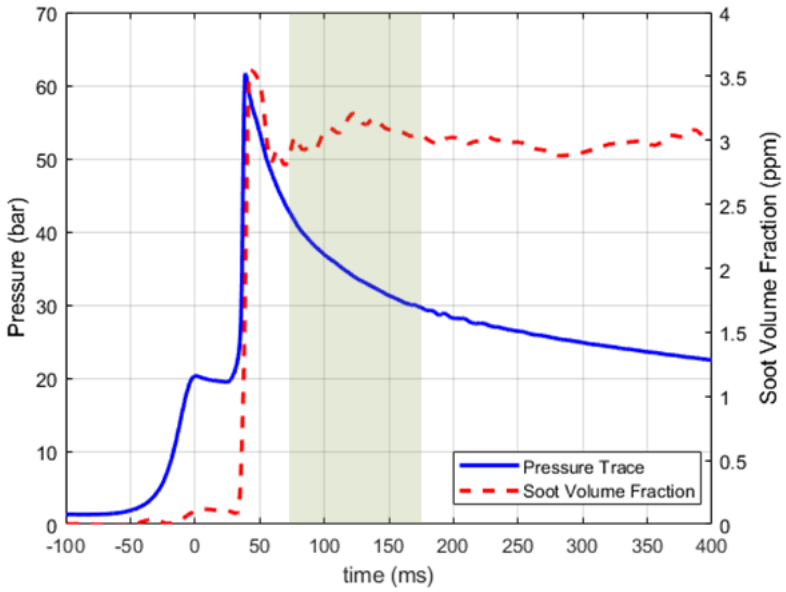

Figure 2.4: Sample data trace for an RCM experiment

Figure 2.4 shows a sample data trace for an RCM experiment. The soot volume fraction data is averaged over a period of 100 ms, starting 25ms after ignition. By comparing the laser transmittance before ignition and after ignition a calculation is made to infer the average soot cloud that must exist for that level of attenuation. For this example trace, the RCM makes around 3 ppm of soot. An

important assumption in this case is that the soot cloud inside the cylinder is assumed to be homogeneous throughout the combustion chamber. The soot volume fraction is calculated using the following equation:

$$SVF(t) = -\frac{\lambda}{k_e L} \log(I(t)/I_o) \tag{2.1}$$

Here, $SVF(t)$ is the soot volume fraction at time t, I_o is the laser transmittance before ignition, and I is the laser transmittance after ignition.

CHAPTER 3

RCM: COMPUTATIONAL MODEL SETUP

This chapter will provide an overview of the computational model and submodels used to simulate the RCM. Tools and software used, along with the various models for all the different components will be discussed in detail. The evolution of the model itself into the current state will also be presented in later chapters. The RCM was simulated using CONVERGE 3.0 with detailed combustion and turbulence modeling.

3.1 Geometry

A detailed 3 dimensional full size geometry of the RCM including the top crevices housing the injector, pressure transducer etc., was created in Autodesk Inventor and exported to CONVERGE as an STL file. Figure 3.1 shows the RCM geometry after import and cleanup. Note the top crevices in the right side of the image.

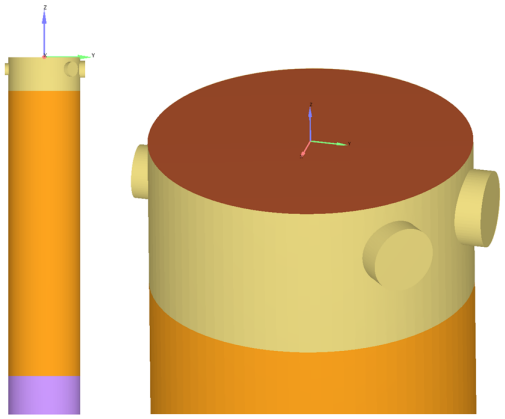

Figure 3.1: RCM CFD geometry with the top crevices

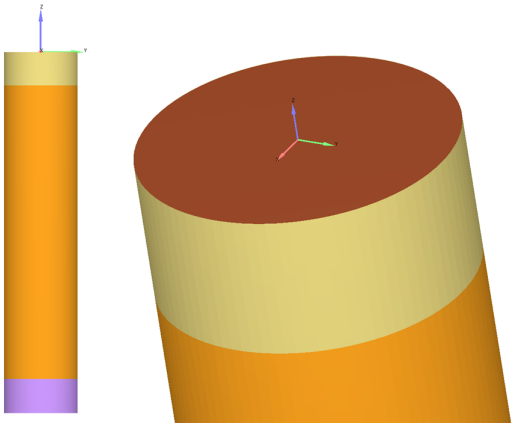

Figure 3.2: Simplified RCM geometry without top crevices

The next step in the development of the geometry was simplifying it in such a way that the experimental nuances would still be captured but at a smaller time cost. With that aim, the crevices in the top of the piston were deleted. To account for the volume of the top crevices, it was added back to the main chamber. This simplified geometry along with the top portion of the deleted crevices is illustrated in the figure 3.2. The validation of the results of all the different geometries will be presented in later sections.

The geometry was then fenced into separate regions called boundaries to prescribe different initialization conditions and mesh settings. The boundaries used for the simulation are highlighted in Figure 3.3.

The geometry was further divided into two regions. With CONVERGE different regions can be defined within the same physical domain to create separate zones with different fluids and thermodynamic properties. In the RCM, the physical domain can be divided into two sections, the crevice region, the regions under the creviced piston which helps with quieting the turbulence associated with compression [57] consisting of the Liner Crevice and Piston Crevice boundaries; and the main region, the combustion chamber above the piston, consisting of all other boundaries. The main region is the main point of

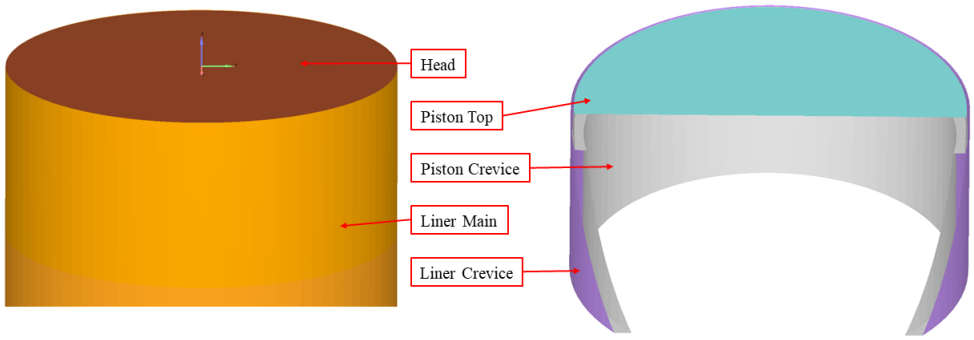

Figure 3.3: Different boundaries of the RCM geometry

interest in our research since combustion takes place in this region. With separate regions we can also define how the simulation works in those regions. In our simulation, since it is a valid assumption that no combustion takes place inside the crevice, the chemistry model was turned off in the crevice region. This saves computational complexity and the time cost for the simulation. Combustion and emissions were turned on in the main region. Although the two regions were separated in terms of chemistry, there was still a physical connection between the two regions through the piston crevice channel. While simulating CONVERGE creates a feature called disconnect triangles between the two regions that allows mass transfer and also the transmission of pressure, temperature and velocity along with the mass transfer.

3.2 Turbulence Model

Turbulence significantly affects the rate of mixing of energy, momentum and species and hence turbulence modeling is critical to obtain accurate simulation results. Turbulence enhanced mixing resulting from turbulent eddies occur at many length scales, currently it is only practical to resolve the bigger length scales and use turbulence models to account for mixing due to the smallest length scales. CONVERGE offers several different turbulence modeling schemes. For this study the Re-Normalization Group (RNG) Reynolds Averaged Navier-Stokes (RANS) k-ϵ model was chosen. Model constants recommended by CONVERGE are used throughout all cases [66].

In this model the Navier-Stokes equations are solved to determine the velocity and pressure fields in the computational domain. The momentum conservation equation is derived by separating the velocity into it's ensemble mean and fluctuating components such as:

$$u_i = \overline{u_i} + u_i{}' \tag{3.1}$$

where u_i is the instantaneous velocity, $\overline{u_i}$ is the mean velocity and u_i' is the fluctuating component of the velocity at that instant. This introduces some unclosed stress tensors, called the Reynolds stresses, containing purely fluctuating components. These terms are not resolved but instead modeled with a turbulent viscosity term which is added to the molecular viscosity in the momentum equation. These models are also sometimes put under the umbrella term two equation models.

3.3 Combustion Model

This study uses the SAGE detailed chemical kinetics solver [68] built into CONVERGE to model combustion. SAGE uses a set of reaction mechanism files formatted in the CHEMKIN style and the CVODE solver. Different fuels can be modeled with different chemical kinetics mechanism. Finding an appropriate mechanism to model gasoline-ethanol blend fuels was one of the primary focus of this study. Each cell in the computational domain is treated as a well stirred homogeneous chemical reactor utilizing CONVERGE's multi-zone scheme. In this scheme, cells are grouped together based on the temperature and equivalence ratio. The temperature is grouped in bin sizes of 5K and the equivalence ratio is binned together in groups of 0.05 bin-width. Grouping together multiple cells in this method contibutes significantly in speeding up the simulation time.

3.3.1 Chemical Kinetics Models

As mentioned, one of the primary focus of this work was discovering an appropriate chemical kinetics mechanisms from the existing library of publicly available mechanisms. Three different detailed and reduced mechanisms were evaluated. The first step was to validate the CFD model against experimental results and subsequently to model soot. The mechanisms used in this study are discussed briefly:

- **Ren Mechanism [65]:** This is a reduced mechanism for wide distillation fuels containing 11 components (n-heptane, iso-octane, toluene, ethanol, methanol, n-decane, n-dodecane, n-hexadecane, diisobutylene, cyclohexane and methyl-cyclohexane) covering six different classes of hydrocarbons. This covers gasoline, jet fuels, diesel and alcohols, which makes it a good choice for simulating different types of fuel under engine like conditions. It

contains 178 species and 758 reactions. This mechanism can be used to predict combustion and soot formations as well as NOx emissions.

- **Andrae Detailed Mechanism [2]:** This is a detailed kinetic mechanism to predict the ignition characteristics of gasoline surrogate fuels. This kinetic mechanism contains 1121 species and 4961 reactions covering 5 components (iso-octane, n-heptane, toluene, diisobutylene and ethanol). This kinetic mechanism was found to accurately predict ignition delay times in shock tube experiments. It can also qualitatively predicts the octane number behaviours for different blends of fuel. This model does not contain any soot inception species but was included in the study to compare against the reduced mechanisms.
- **Kalvakala Mechanism [37]:** This is a reduced kinetic mechanism proposed for numerical analysis of soot formation from gasoline and biofuel blend fuels such as gasoline-ethanol or gasoline-butanol blends. This mechanism can describe the chemistry of n-heptane, iso-octane, n-butanol, ethanol, and toluene and contains 273 species and 1637 reactions. It also incorporates PAH chemistry for detailed soot formation calculations.

3.3.2 Fuel Surrogate

Real fuels such as gasoline or diesel, are a complex mixture of an almost continuous spectrum of hydrocarbons. They are also affected by the source and refining processes which make it tremendously difficult to ascertain the exact molecular mixture of a real fuel. Hence a common practice in computational modeling is the use of a surrogate fuel which is a known blend of a finite number of selected species. This surrogate fuel exhibits similar combustion characteristics of the real fuel under investigation.

In the experiments a 85 AKI BOB (Blendstock for Oxygenate Blending) gasoline was splash blended with fuel grade denatured ethanol to create the gasoline-ethanol blend fuels. Different levels of ethanol blends were investigated, market existing e10 and e85, pure ethanol e100 and a middle of the road e30 blends were tested in the experiments. Some specifications for the experimental gasoline BOB are detailed in table 3.1.

Table 3.1: Gasoline BOB Specifications

HC Class	**Amount**
Aromatics	8.1%
Olefins	4.5%
Saturates	87.4%
Property	**Value**
RON	87.00
MON	82.60
AKI	84.80

The gasoline BOB had 3 specified components, saturates, olefins and aromatics. For the Ren and Andrae chemical mechanisms the aromatics were modelled as Toluene, the saturates were modelled as a mixture of iso-octane and n-heptane and the olefins were modelled as di-iso-butalyne. The kalvakala mechanism did not contain any olefins so the olefin content was replaced with the saturates and modelled as a Toluene Primary Reference Fuel(TPRF). The fuel grade ethanol was modelled as pure ethanol for the blended gasoline-ethanol fuels. Some properties of the surrogate gasoline fuel used with the Kalvakala mechanism are presented in table 3.2. The ratio of n-heptane and iso-octane in the saturate content can be adapted to adjust the experimental ignition delay. The surrogate fuels were generated in a way to have closest matches to the combustion characteristics as well as some of the properties. CONVERGE's

Table 3.2: Surrogate Fuel Specification for Kalvakala Mechanism

HC Species	**Amount**
$C_6H_5CH_3$	8.1%
NC_7H_16	21.9%
IC_8H_18	70.0%
Property	**Value**
RON	82.90
MON	80.59
AKI	81.75

built-in chemistry tools were used to find the properties of surrogate fuel used in the models. In house blending tools built with MATLAB were used to prepare the gasoline-ethanol blends at different mixing levels as well as to prepare the charge at different equivalence ratios.

3.4 Mesh

One of the most critical components of CFD modeling is making a suitable mesh. The mesh in a CFD model is the collection of cells in the geometry itself. CONVERGE has fully automated mesh generation which makes it quite easy to build an appropriate mesh for a given geometry. There are still some user defined mechanisms to optimize and refine the mesh as necessary. In this study two such tools, adaptive mesh refinement and fixed embedding was used to increase the fidelity of the geometric model. The base grid size was fixed at 2mm for all the cases. An example of the mesh alongside the various refinement is illustrated in figure 3.4. Details about the mesh settings used for this study are mentioned later in Table 4.3.

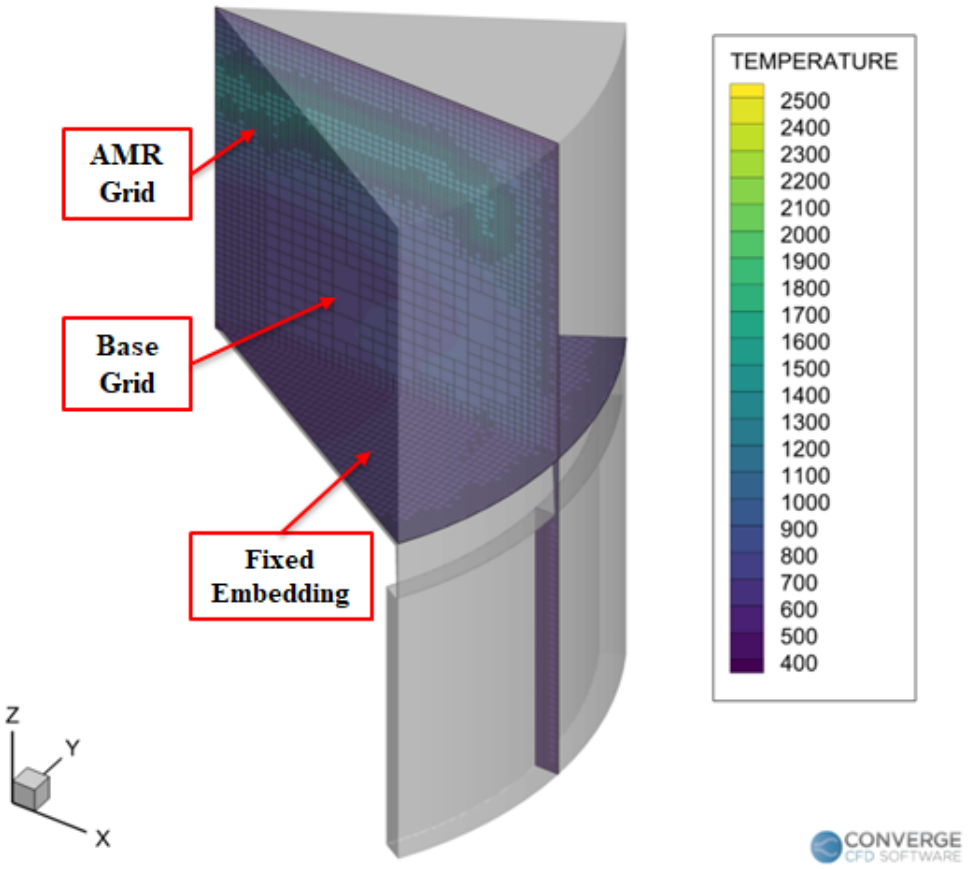

Figure 3.4: RCM Simulation Mesh

3.4.1 Adaptive Mesh Refinement

Adaptive mesh refinement (AMR) is a technique where the mesh is automatically refined based on defined property gradients in and around the computational cell. In this study, AMR was done based on temperature and velocity gradients. If the temperature or velocity gradient in a local mesh was higher than the sub-grid criterion, the mesh was refined (i.e., made smaller in size) in that location. As the gradients dropped off below the criterion the mesh was coarsened up to the base grid size. The max embedding level defined the level of refinement by defining how small could a cell be made. In the current study a max embedding level of 3 was used for both temperature and velocity

along with a sub-grid criterion of 2.0 K for temperature and 1.5 m/s for velocity.

3.4.2 Fixed Embedding

With CONVERGE's fixed embedding feature, finer mesh grids can be made in specific areas of interest in the simulation domain. Fixed embedding are fixed in space and can be permanent throughout the simulation or temporally defined. The embedding scale defines how the refinement is done at that location. The final grid size at a fixed embedding is given by:

$$embed\_grid = base\_grid/2^{embedding\_scale} \tag{3.2}$$

In this study, fixed embedding was defined for all boundaries of interest. The embed scaling of the fixed embedding scheme is detailed in Table 4.3.

3.5 Emissions Model

CONVERGE has several different models for calculations of NOx and particulate matters or soot emissions. Other emissions species of interest such as CO, CO_2, unburned hydrocarbons etc. are calculated through the combustion models, given that these species exist in the mechanism. In this project the primary interest for emissions is on soot for different gasoline-ethanol blend fuels. Detailes about NOx modeling or other species can be found in the CONVERGE 3.0 manual [66].

3.5.1 Soot models

There are multiple options in CONVERGE for modeling soot starting from simple empirical models to more complex models that model the physical phenomenon of soot formation,growth and oxidation along with the interaction between soot and chemistry. In this research project to frame the current stare of

soot mdoelling capabilities the two bookend models available in CONVERGE was used. The simplest available model Hiroyasu and the most detailed model Particulate Size Mimic. There are also phenomenological models available in CONVERGE but no such models were evaluated in this study. The models were evaluated in their default configuration and then they were tuned via various available model parameters to improve the agreement with the experiments.

3.5.1.1 Hiroyasu-NSC Model

The simplest soot model available in CONVERGE 3.0 is the Hiroyasu-NSC two step model, the only empirical soot model available. The Hiroyasu emperical model is coupled with the Nagle and Strickland-Constable Model [60] to simulate soot oxidation. This model basically consists of two competing processes, soot formation and soot oxidation. This model does not interact with the combustion chemistry model. It also does not consider soot surface growth processes or particle coagulation.

According to Hiroyasu and Kadota [32] the rate of soot generation (M_s) n a computational cell is calculated from the difference between the soot formation (M_{sf}) and soot oxidation (M_{so}) rates.

$$\frac{dM_s}{dt} = \frac{dM_{sf}}{dt} - \frac{dM_{so}}{dt} \tag{3.3}$$

The formation rate can be expressed as a pressure dependent Arrhenious expression as follows

$$\frac{dM_{sf}}{dt} = A_{sf} M_{form} P^{0.5} exp(\frac{-E_{sf}}{RT}) \tag{3.4}$$

here A_{sf} is the Arrhenius pre-exponential factor with units of $s^{-1} - bar^{-0.5}$, M_{form} is the mass of the soot formation species in *grams* predicted by the combustion chemistry, P is the local cell pressure in *bar*, E_{sf} is the activation energy in *cal/mol*, R is the ideal gas constant in *cal/mol-K*, and T is the local cell temperature in *K*.

The soot formation species has two options that can be defined by the user, the first option uses the total hydrocarbon mass from the fuel vapor as the soot formation species mass. The second option only uses acetylene (C_2H_2) as the soot formation species. Using this option requires the use of a detailed chemistry solver like the SAGE detailed chemical kinetics solver used in this study. This study uses acetylene as the soot formation species as previous research has acetylene is an important soot precursor species [74]. Additionally with the use of detailed kinetics, fuel vapor is rapidly transformed into intermidiate hydrocarbon species [45].

With this model in CONVERGE, soot oxidation is modeled using the Nagle and Strickland-Constable model. This model considers carbon oxidation through two mechanisms dependent on surface chemistry at two sites, the more reactive A site, and the less reactive B site.The total rate of soot oxidation is given as:

$$\frac{dM_{so}}{dt} = A_{so}\frac{6MW_c}{\rho_s D_s}M_s R_{ox} \tag{3.5}$$

Here, A_{so} is a scaling factor for soot oxidation, MW_c is the molecular weight of carbon in *g/mol*, ρ_s is soot density in g/cm^3 and D_s is the soot particle diameter with units of μm. The soot density, ρ_s is set to 2 g/cm^3 and the soot diameter, D_s was set at 0.25 μm for this study following the prescribed settings in CONVERGE.

R_{ox} is the total soot oxidation rate given by,

$$R_{ox} = (\frac{K_A P_{O_2}}{1 + K_Z P_{O_2}})X + K_B P_{O_2}(1 - X) \tag{3.6}$$

where X is the proportion of A sites as given by

$$X = \frac{P_{O_2}}{P_{O_2} + (k_T/k_B)} \tag{3.7}$$

In the above equations, P_{O_2} is the local cell oxygen partial pressure in *atmospheres* and the k values are rate constants. The k values were set to the

default and can be found in the CONVERGE manual.The only soot oxidizer in this model is oxygen, which is a deficiency of the two-step model.

3.5.1.2 Particulate Size Mimic Model

The Particulate Size Mimic (PSM) is the most advanced soot model implemented in CONVERGE 3.0. This model was developed based on the discrete sectional method [46,78]. This model provides the particle size distribution function (PSDF) of each cell in addition to the detailed soot information such as cell averaged soot number density and mass. The PSM model divides the particles into bins, called sections in CONVERGE, containing particles of similar volume. The first bin is populated through nucleation of soot particles. The particles can then move from one bin to another depending on the changing size of the particles through surface growth, condensation, coagulation, oxidation or fragmentation. The boundaries of each section is given by:

$$\begin{aligned} v_{1,min} &= v_{MIN} \\ v_{1,min} &= v_{i-1,max}, \text{ for } i > 1 \\ v_{i,mean} &= \frac{v_{i,min} + v_{i,max}}{2} \end{aligned} \tag{3.8}$$

For increased computational efficiency, the maximum boundary is extended using the a nonlinear formulation [62] given by:

$$\begin{aligned} v_{1,max} &= v_{min} + v_{C2} \\ v_{i,max} &= (v_{min} + v_{C2})(\frac{v_{MAX}}{v_{MIN} + v_{C2}})^{\frac{i-1}{i_{max}-1}} \end{aligned} \tag{3.9}$$

Here v_{MIN} is the minimum volume defined by the soot precursor, which can be specified by the user. The maximum soot volume, v_{MAX} is preset by CONVERGE as the biggest soot particles with an approximate diameter of 100 nm. The maximum volume of the biggest soot particle can also be specified by the user. v_{C2} is the volume of two carbon atoms in soot calculated to be 7.176e4 nm^3.

Given the distribution function $q_i(v)$ for each section, the total volume fraction Q_i is:

$$Q_i = \int_{v_{i,min}}^{v_{i,max}} q_i(v)dv \tag{3.10}$$

Following equation 3.10 soot formation in each section in the PSM model is calculated by the following equation where $\dot{S}_{Q_i}$ is the source term:

$$\dot{S}_{Q_i} = \Delta\dot{Q}_{i,pi} + \Delta\dot{Q}_{i,sg} + \Delta\dot{Q}_{i,ox} + \Delta\dot{Q}_{i,coag} + \Delta\dot{Q}_{i,con} \tag{3.11}$$

Here, $\Delta\dot{Q}_{i,pi}$, $\Delta\dot{Q}_{i,sg}$, $\Delta\dot{Q}_{i,ox}$, $\Delta\dot{Q}_{i,coag}$, $\Delta\dot{Q}_{i,con}$ refer to the rate of particle inception, surface growth, oxidation, coagulation, and condensation. The section source term is coupled with the species source terms in a two-way coupling and solved using the SAGE detailed chemical kinetics solvers. This results in the soot formation affecting the gas phase and system heat release and vice-versa. The detailed formulation for each of the rates can be found in the CONVERGE 3.0 manual [66].

3.6 Initialization

The RCM CFD simulation initialization was done at similar conditions as the experiment being simulated aiming at achieving the same compressed temperature and pressure conditions. It was assumed that the wall temperatures were at the set point defined in the experiment. The gas inside the RCM itself was assumed to have a homogenous distribution of mixture, temperature and pressure. An in-house Python processing tool was used to calculate the mass fractions of the gas mixture components from the experimental measurements of fuel mass injected and air mass inside the cylinder.

In the RCM experimental setup the piston is moved hydraulically along a cam. The stroke length is fixed at 8 inches or 0.2032 metres. One of the first challenges in building the CFD model was simulating the piston movement as

closely as possible. A piston movement profile from previous research [79] was taken as the baseline model and a improved profile was created. The experiment had the capability of changing the driving pressure of the piston which would change the piston movement profile but since the compression ratio and thermodynamic property at top dead centre was the main point of concern, the slight variations resulting from different driving pressures were not simulated and a constant piston movement profile was assumed.

CHAPTER 4

MODEL DEVELOPMENT AND RESULTS

This chapter will discuss the development and evolution of the computational simulation model to the current state. Design decisions taken at each step of the process will be explored and explained. The effect of the various settings in the models will also be illustrated. Finally, the results from the study of different soot models and chemical kinetics mechanisms will be discussed in this chapter. The evolution of the model is presented as chronologically as possible, but in some cases, multiple developments were made in the same timeline. The final state of the model will be presented before discussing the final results.

4.1 Model Validation

The computational model was validated against the experimental data by comparing the pressure trace data and the ignition delays of the different fuels at different equivalence ratios. Figure 4.1 shows an example data trace from a CFD model for E30 fuel at an equivalence ratio of 1.5. The CFD model closely follows the compression process of the RCM. It also does a good job of capturing heat transfer losses post compression before ignition. The ignition delay is also well predicted as the pressure rise rates take off at the same time as the experiments. This plot shows several replicates taken at this condition to illustrate the repeatability of the RCM experiments. One thing were the CFD model does a poor job is predicting the peak combustion pressure. The peak pressure is higher than the experiments by a margin of 10 bars or about 14%. This discrepancy was investigated in detail in trying to improve the models prediction. Existing research does show that RCM CFD models have trouble with overpredicting the peak combustion pressure as shown by Gholamisheeri et. al [26].

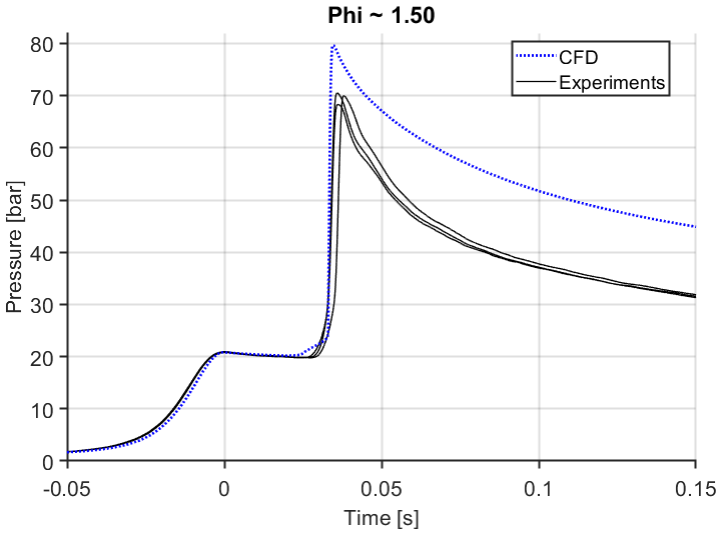

Figure 4.1: Example data trace from the CFD Model

The ignition process was also looked at closely to see the development of the combustion in-cylinder. Figure 4.2 illustrates the combustion process inside the RCM in at various timesteps after reaching Top Dead Center (TDC). The initial combustion starts at the upper portion of the cylinder and then progresses to the outer periphery before engulfing the center. This step-by-step combustion process inside the RCM is supported by existing literature [12,30,77] and further validates the CFD model. As the piston is compressed a cold plug of gas is pushed into the center which creates a temperature stratification at the core of cylinder which affects the reaction speed. This results in the combustion developing in a toroidal manner as seen in the CFD model.

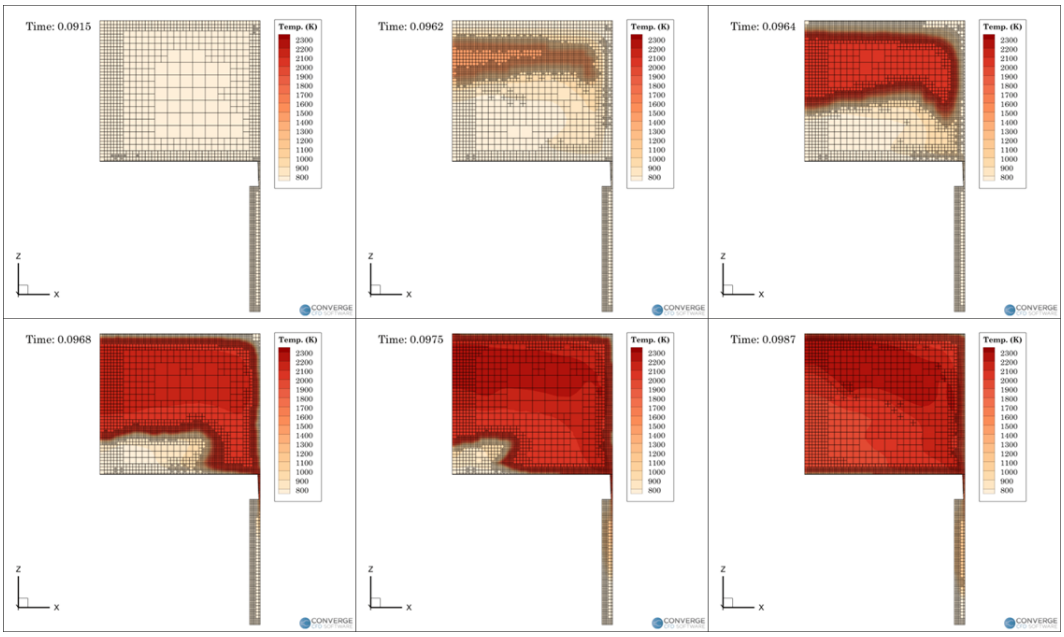

Figure 4.2: Progression of combustion in the RCM CFD model after reaching TDC

Based on the primary results, investigative modifications were made to the model to improve the prediction capabilities. These modifications and their implications are discussed in the following sections.

4.2 Combustion Modeling in Crevice Region

Initially, to resolve the peak pressure discrepancy issues, combustion in crevice region was investigated. In the initial model, the combustion modeling was enabled for the whole computational domain. The higher peak pressure was thought to be resulting from combustion occurring in the crevice region. In the experiments, a assumption is made that the crevice region is too cold from absorbing the boundary layers to have any combustion events. The CFD model was unable to predict this and predicted combustion events happening in the crevice region. This led to the crevice region acting like a prechamber with hot combustion products transferring into the main chamber and affecting the overall

combustion pressure. To resolve this issue, combustion events in the crevice region was turned off to keep in line with the experimental assumptions. Figure 4.3 shows the pressure traces and heat release rates for cases comparing combustion modeling in crevice vs no combustion in the crevice region. The

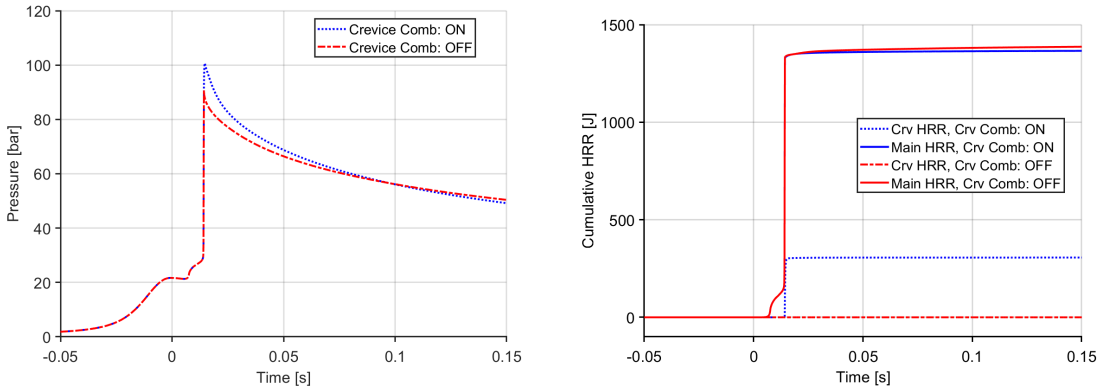

(a) Main Chamber Pressure Traces (b) Cumulative Heat Release Rates

Figure 4.3: Comparison between cases with combustion modeling in Crevice region on and off

figures show that there is very little difference in the total heat release rates for the main chamber whether or not combustion in the crevice is turned on but it significantly affects the peak combustion pressure.

4.3 Geometry effects

4.3.1 Sector Geometry

The RCM is was axially symmetric and the combustion process inside the is assumed to be completely homogeneous, hence to reduce resource costs the RCM model was further simplified by dividing it into sectors. With CONVERGE 3.0 cylindrical geometries can be sliced much like pie slices into sectors, the two side surfaces of the slice must exactly match each other, i.e. have the same

perimeter geometry; these surfaces are called periodic boundaries. During the simulation, the boundary conditions of one of these periodic surfaces are copied over to its matching boundary [66]. For a 180° model the boundary is named a symmetry. Two sector geometries with sector sizes of 60° and and 180° were prepared and tested. With the axisymmetric homogeneity assumption, an argument can be made for even smaller sector sizes in order to cut down on resource expenses, hence, two other smaller sectors of 30° and 10° were also prepared. These sectors had major disagreements compared to the experiments and other sector geometries. In the interest of time and progress, these sectors were not further validated. Figure 4.4 shows the two geometries evaluated. Figure 4.4a shows the 60° CFD geometry where the red face denotes one of the periodic boundary. In figure 4.4b the 180 model is illustrated with the red face denoting the boundary of symmetry.

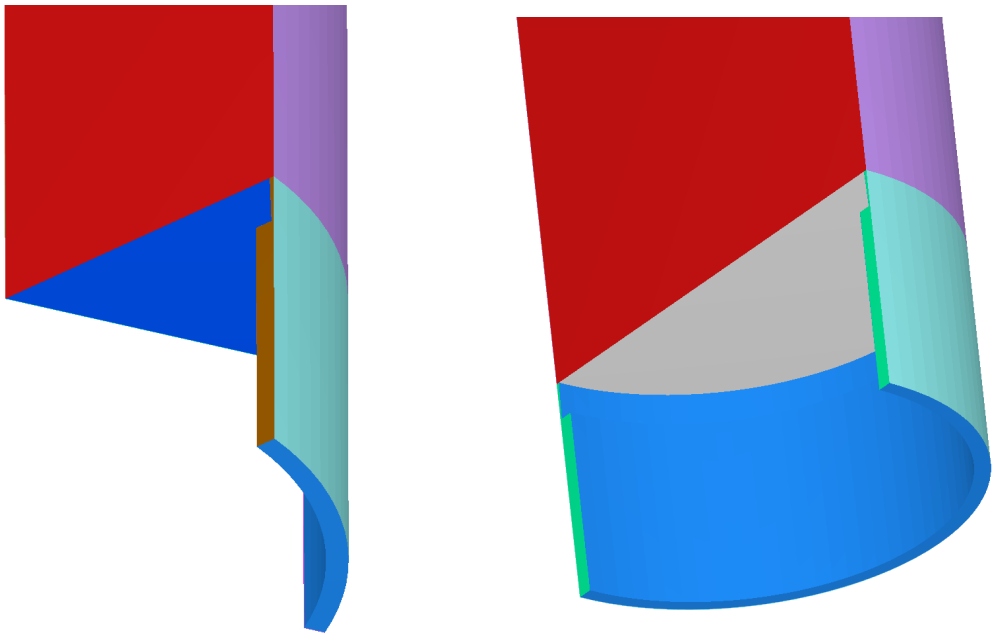

(a) 60° RCM CFD Geometry (b) 180° RCM CFD Geometry

Figure 4.4: Case results with different sector geometries

The sector models as well as the simplified 360 degree model was compared to the results from the detailed geometry and validated against the experimental data. Figure 4.5 shows the results of these cases. All three models show very good agreement. The 60° model has the best balance between accuracy of results and resource cost for modeling as it needed less half the time to run as compared to the full size model and 40% less time compared to the 180° model. Thus the 60° sector model was chosen to be used for all future simulations. It is also of note the bulk gas temperature distribution in the main chamber as illustrated in 4.5c.

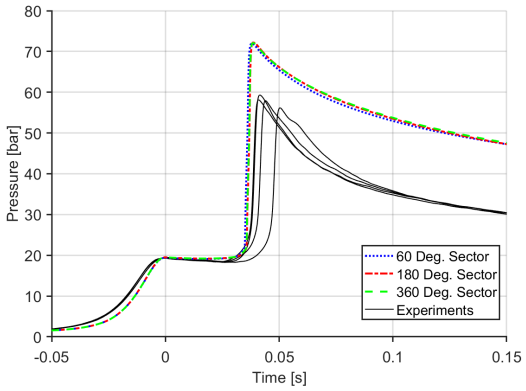

(a) Main Chamber Pressure Traces

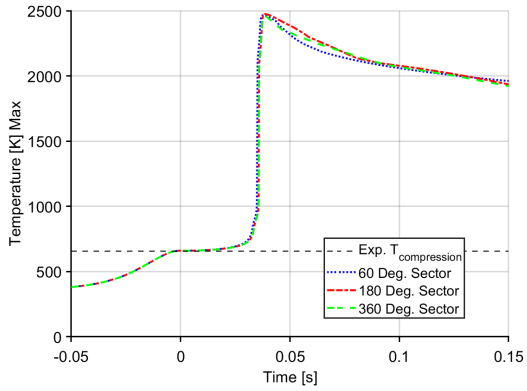

(b) Max Temperature in Main Chamber

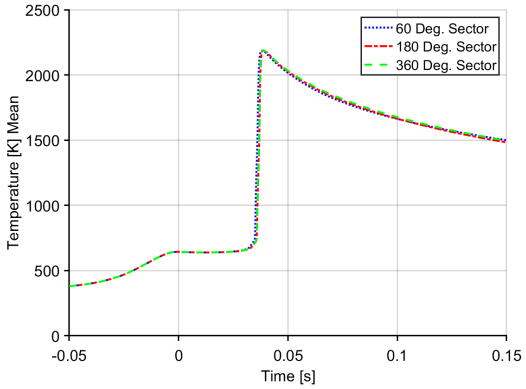

(c) Mean Temperature in Main Chamber

Figure 4.5: Case results with different sector geometries

4.3.2 Crevice Geometry

The interaction between the crevice and main chamber is one of the critical components of the RCM model. In the experimental setup it is assumed that the crevice minimizes the boundary layer effects in the main chamber thus helping the homogeneous core assumption. To observe the effect of the crevice volume itself as well as the channel between the crevice and the main chamber several different cases were run with differing crevice geometries. Since the model over predicts peak combustion pressure, a larger crevice volume and a larger crevice channel was investigated to see if the increased mass flow into the crevice helped resolve this discrepancy.

- **Larger Crevice Channel:** The size of the crevice channel was increased from 0.38 mm to 1.38 mm. The effect of the larger crevice channel is illustrated in in figure 4.6. The larger crevice channel resulted in very similar compressed pressure and temperature but had an increased ignition delay. This can be caused more mass flow between the main chamber and the crevice which decreases the total amount of fuel energy in the main chamber.

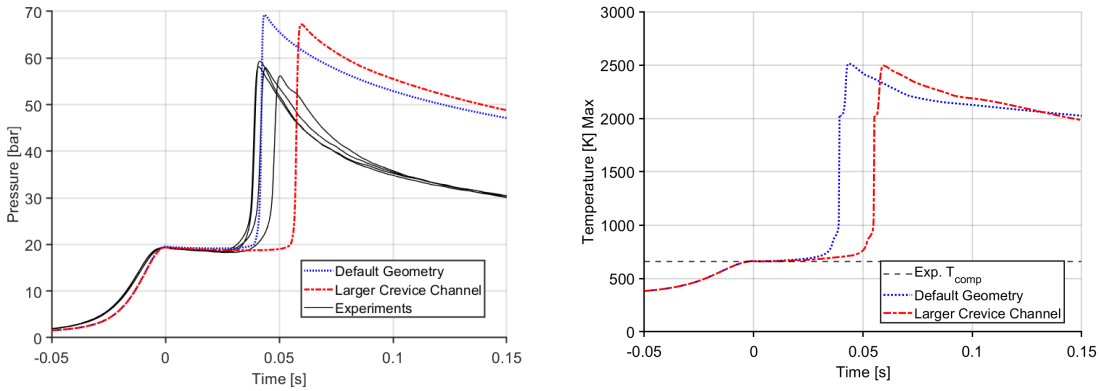

(a) Main Chamber Pressure Traces (b) Max Temperature in Main Chamber

Figure 4.6: Case results with larger crevice channel compared to default geometry

- **Larger Crevice Volume:** The size of the crevice volume was increased by 20% from an initial volume of 8.87e-7 mm^3 to 10.06e-7 mm^3. The main chamber volume was adjusted accordingly to maintain the same compression ratio. The increase in the crevice volume results in a slightly lower peak combustion pressure along with delayed ignition. This is highlighted in figure 4.7

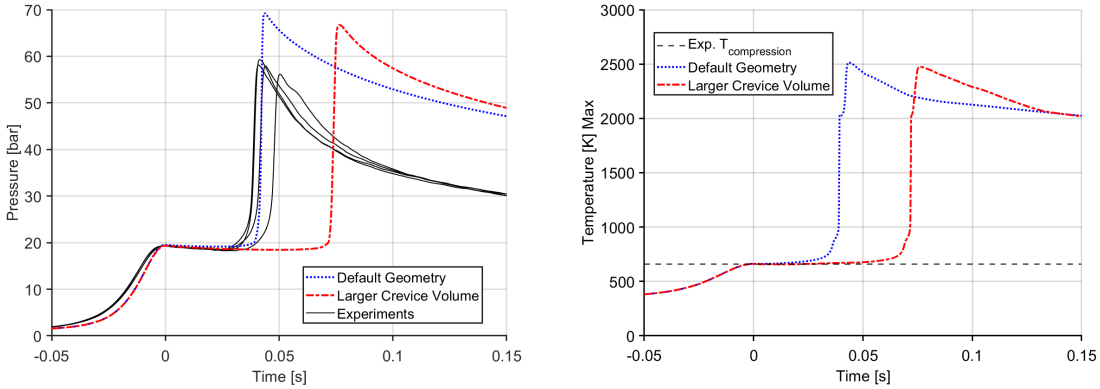

(a) Main Chamber Pressure Traces (b) Max Temperature in Main Chamber

Figure 4.7: Case results with larger crevice volume

The effects of changing the crevice geometry was not satisfactory in resolving the peak pressure delta and reduced the models accuracy in predicting the ignition delay. Both of these designs were scrapped and the default geometry was chosen to be used from here on forward.

4.3.3 Fixed Embedding Improvements

In order to improve the resolution of flow through the crevice channel, the fixed embedding settings were changed, introducing finer and more layers of embedding in the geometry. The improved mesh resulted in a slight advancement of ignition. This is highlighted in figure 4.8. With the finer mesh

there was an improvement in the creviced pistons ability in scooping up the boundary layer which improved the ignition event prediction. The finer mesh settings does introduce an increased resource cost but the improvement in the model's fidelity was seen to be a necessary step up.

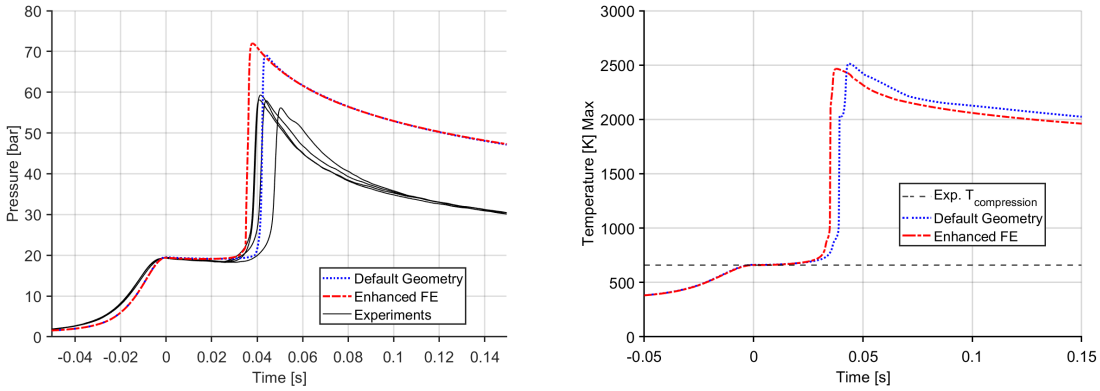

(a) Main Chamber Pressure Traces (b) Max Temperature in Main Chamber

Figure 4.8: Case results with improved fixed embedding mesh in the crevice region

4.4 Mechanism Evaluations

As mentioned in section 3 three mechanisms were primarily evaluated; the detailed Andrae mechanism [2] and the two reduced mechanisms by Ren et. al. [65] and Kalvakala et. al. [37]. Since the Andrae mechanism did not have any soot precursor species, a primary run with no soot models was done to validate the ignition chemistry of the three models. The results form this trial is illustrated in figure 4.9. This trial run was done with the E30 fuel at a equivalence ratio of 2.2. Out of the three mechanisms the Kalvakala mechanism had the best agreement with the experimental data. Even though the Andrae mechanism is a detailed mechanism, it had the longest ignition delay. Due to the longer ignition delay predictions along with the unavailability of soot precursors, this

mechanism was excluded from any further investigations.

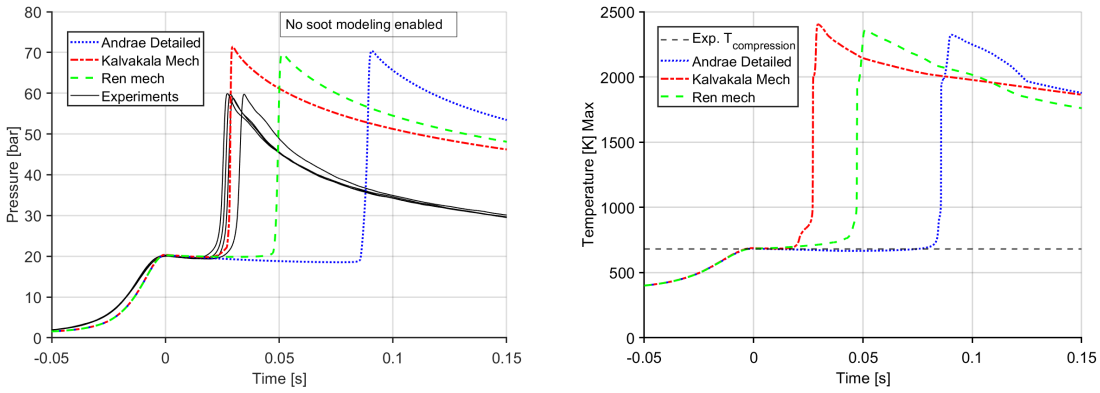

(a) Main Chamber Pressure Traces (b) Max Temperature in Main Chamber

Figure 4.9: Case results comparing different chemical kinetic mechanisms [No Soot Modeling]

The two remaining mechanisms, the Ren mechanism and the Kalvakala mechanism, were then evaluated with the PSM soot model turned on to see if there were any effects of the detailed soot model in the ignition chemistry. Since the PSM model interacts with the chemistry model but the Hiroyasu model does not, this was an important factor to understand the overall accuracy of the model with different soot models. The PSM soot model had no significant effect on the ignition chemistry of the Kalvakala model but the cases running the Ren mechanism was significantly affected by it. Given the accuracy in predicting ignition delay times as well as not being affected by the presence of detailed soot models, the Kalvakala mechanism was chosen to be used on subsequent modeling.

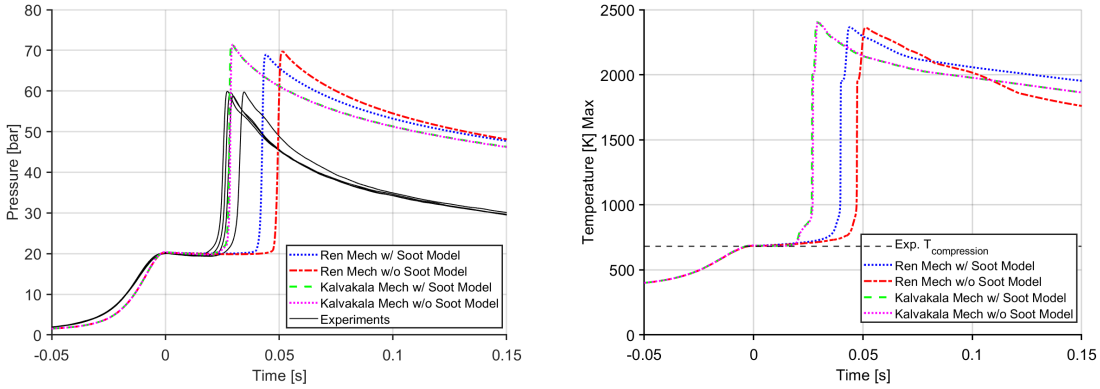

(a) Main Chamber Pressure Traces (b) Max Temperature in Main Chamber

Figure 4.10: Case results comparing different chemical kinetic mechanisms with and without soot modeling

4.5 SAGE Model Multiplier Effects

Another approach in understanding the high combustion peak pressures in the CFD model investigation into understanding how the chemistry model may have been affecting the peak pressure. The combustion model SAGE offers a multiplier that can be changed to increase or reduce the overall reactivity of the chemical kinetics mechanisms in the model. This multiplier was turned down in two 5% increments to ascertain the effect on peak combustion pressure as well as ignition chemistry. Figure 4.11 shows the effect of the SAGE model multiplier on the combustion in the CFD model. The reduction of the multiplier has little to no effect on the peak combustion pressures but has an appreciable effect on the ignition delay although quite minor. Since upto 10% reduction in the multiplier did not have a major effect on the peak combustion pressure, the combustion model was understood to not affect the peak pressure in any significant way.

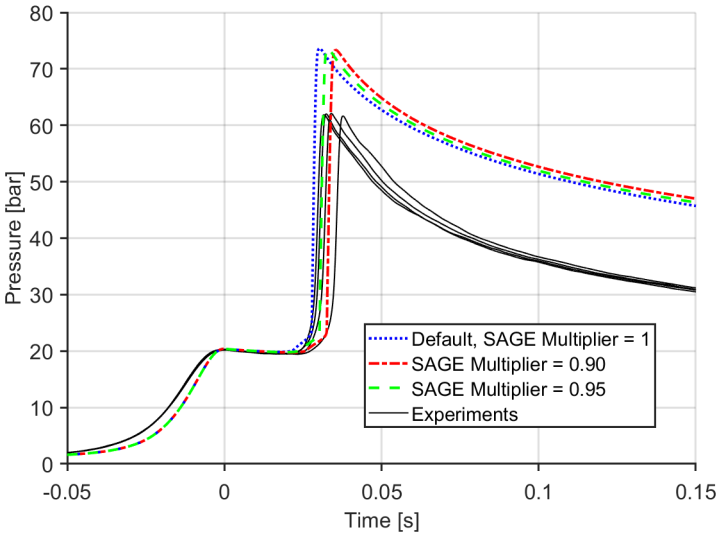

Figure 4.11: Main Chamber Pressure Traces for different SAGE Model Multipliers

4.6 Soot Model Parameter Sweep

The two soot model being evaluated both have some parameters that can be changed by the user. A systematic parameter sweep of some of these parameters were done in order to understand the effect of these parameters as well as to increase the models capability in predicting soot. The following sections will discuss the parameter sweeps and their results as well as highlight the final settings that were used for the current simulation model.

4.6.1 Hiroyasu-NSC Model

The empirical Hiroyasu-NSC model is quite tunable. Different factors can be defined by the user to change the soot yield in the simulation. In this case the the Arrhenius pre-exponential factor, A_{sf}; the activation energy, E_{sf} and the oxidation scaling factor, A_{so}; were parametrically swept to affect soot yield. Table 4.1 lists the sweep cases and the values of the different factors evaluated. All of these trial cases were run with E30 fuel at an equivalence ratio of 2.0 Since the

Hiroyasu model does not affect the chemistry model, the experimental pressure trace is the same for all the cases. Figure 4.12a illustrates this fact.

Table 4.1: Parameters swept for the Hiroyasu-NSC Model

Hiroy	$\mathbf{A_{sf}}$	$\mathbf{E_{sf}}$	$\mathbf{A_{so}}$
Default	**350**	**12500**	**1**
Case 1	350	**10000**	1
Case 2	350	**7500**	1
Case 3	**450**	12500	1
Case 4	**550**	12500	1
Case 5	350	12500	**0.5**
Case 6	350	12500	**0.25**
Final	**550**	**6000**	**1**

- **Activation Energy, $\mathbf{E_{sf}}$:** Effect of the activation energy was the most substantial. Decreasing the ESF increases soot yield. This parameter was swept from a default value of 12500 to 7500 in two steps of 2500. The steps were chosen arbitrarily. The effect of this factor is illustrated in figure 4.12b.
- **Arrhenius pre-exponential factor, $\mathbf{A_{sf}}$:** The formation rate factor had a significant effect on soot yield but it less prominent compared to the activation energy. Figure 4.12c shows the increase of soot yield due to the increase of the Arrhenius factor compared to the default case.
- **Oxidation factor, $\mathbf{A_{so}}$:** The oxidation factor had little effect on the soot yield compared to the default as shown in figure 4.12d. Since the RCM experiments and simulations were run at fuel rich conditions the soot formation reaches a steady state post combustion due to lack of excess oxygen. The lack of effects of the soot oxidation factor leads credence to this observation.

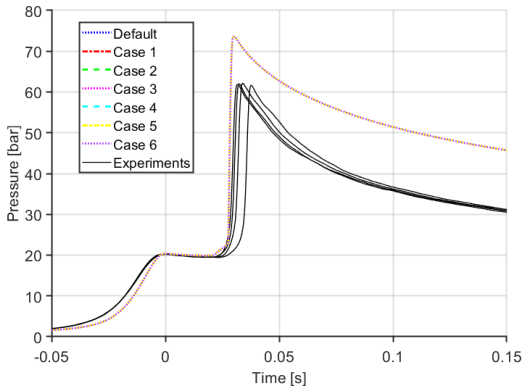

(a) Main Chamber Pressure Traces

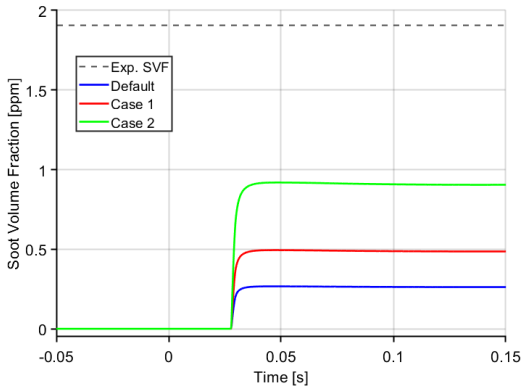

(b) Soot Volume Fraction vs Time

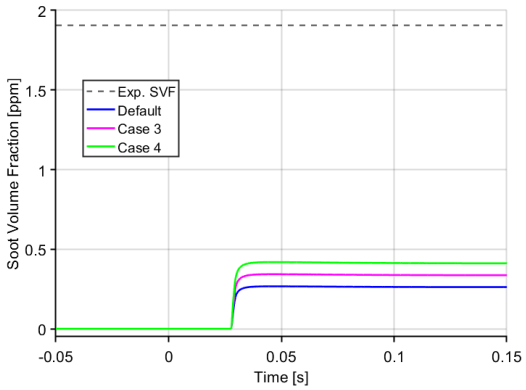

(c) Soot Volume Fraction vs Time

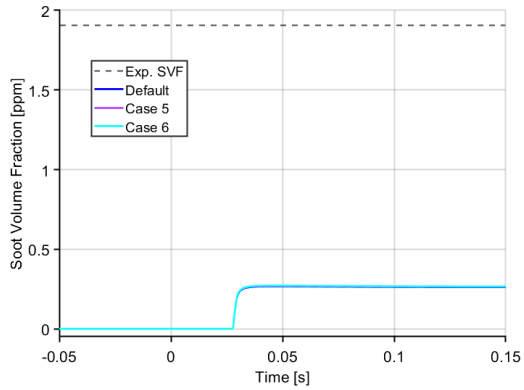

(d) Soot Volume Fraction vs Time

Figure 4.12: Hiroyasu-NSC model parameter sweep results

Based on the trials with the different factors, a final value of $\mathbf{A_{sf}} = 550$, $\mathbf{E_{sf}} = 6000$, and $\mathbf{A_{so}} = 1$ was chosen as the tuned case parameter. Figure 4.13 illustrates the soot yield for this final case compared to the default values. As expected, the pressure trace is not affected by changes in the Hiroyasu model. The final chosen parameters do yield slightly more soot than the experimental calculations but for the sake of brevity, these parameters were chosen to be used in future modeling RCM cases.

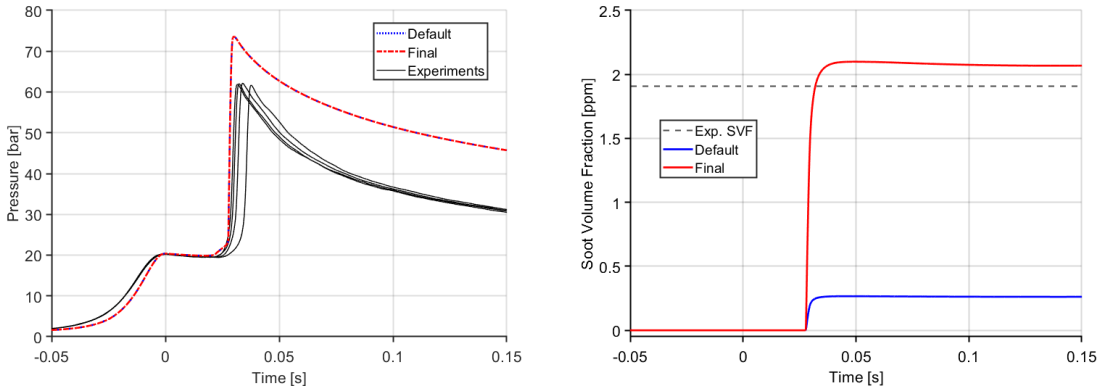

(a) Main Chamber Pressure Traces (b) Soot Volume Fraction vs Time

Figure 4.13: Comparison of default and tuned Hiroyasu Model Soot Yield

4.6.2 Particulate Size Mimic

The detailed Particulate Size Mimic(PSM) model does not have many user changeable parameters, in that sense this model is less "tunable" than the Hiroyasu-NSC model. There are still some parameters that can be defined by the user and these were evaluated systematically in this study. The first such parameter that was evaluated is the α correction factor for surface reactions.

CONVERGE uses the Hydrogen Abstraction Acetylene Addition Ring Closure (HACARC) [52]. Recalling section 3.5.1.2, the surface reactions rate's for surface growth and oxidation are $\Delta\dot{Q}_{i,sg}$, $\Delta\dot{Q}_{i,ox}$ respectively. These are computed as the following equations [51, 66]:

$$\begin{aligned}\Delta\dot{Q}_{i,sg} &= \alpha v_{c2}^{\frac{3-\theta}{3}}(k_d - k_{rev})\left(\frac{3}{3+\theta}q_i\left(v_{i,max}^{\frac{3+\theta}{3}} - v_{i,min}^{\frac{3+\theta}{3}}\right) + \frac{3}{\theta}q_i^{\mu}\left(v_{i,max}^{\frac{\theta}{3}} - v_{i,min}^{\frac{\theta}{3}}\right)\right)\\ \Delta\dot{Q}_{i,ox} &= \alpha v_{c2}^{\frac{3-\theta}{3}}(k_{O2} - k_{OH})\left(\frac{3}{3+\theta}q_i\left(v_{i,max}^{\frac{3+\theta}{3}} - v_{i,min}^{\frac{3+\theta}{3}}\right) + \frac{3}{\theta}q_i^{\mu}\left(v_{i,max}^{\frac{\theta}{3}} - v_{i,min}^{\frac{\theta}{3}}\right)\right)\end{aligned} \tag{4.1}$$

Here θ is the fractional dimension of soot and k is the reaction rate coefficient specified in Marchal [51] and α is the fraction of soot surface site utilized for these surface reactions ranging from 0 to 1. For the PSM model, this factor is defined

based on the size of the soot particle. Soot sizes from precursor species up to 40nm size is binned with the first factor and particles bigger than 40nm is binned at the second alpha correction factor. For this study, only the second alpha correction factor was evaluated. CONVERGE also allows the alpha correction factors to automatically calculated based on local conditions.

The second factor that was evaluated for the PSM model is defining custom soot precursors. This model allows the user to define the species that will be used as a precursor for soot inception and growth. Starting with the biggest PAH (polycyclic aromatic hydrocarbon) available with the Kalvakala mechanism, Cyclopenta-Pyrene (A4R5), smaller PAHs are progressively added to illustrate the effect of custom precursor definitions on overall soot yield. Figure 4.14 highlights the PSM model settings for alpha correction factors and custom soot precursors. Table 4.2 listed the different settings for the parameter sweep of the PSM model.

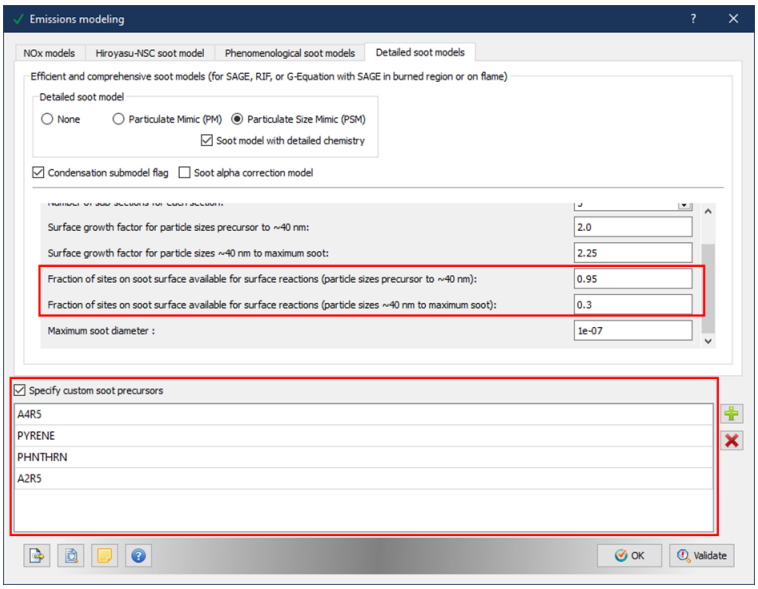

Figure 4.14: Settings for the PSM soot model

Table 4.2: Parameters evaluated for the PSM model

PSM	α_2	**Inception Species**
Def	**Auto**	**A4R5**
Case 1	**0.5**	A4R5
Case 2	**0.7**	A4R5
Case 3	**0.9**	A4R5
Case 4	Auto	**A4R5+A4**
Case 5	Auto	**A4R5+A4+A3**
Case 6	Auto	**A4R5+A4+A3+A2R5**

Figure 4.15 shows the effects pf the α correction factor. With higher second alpha corrector factor the soot oxidation reactions become more prominent causing the soot yield to drop after peaking at combustion initiation. This is also evident from the decrease in soot mass as highlighted in Figure 4.15c. For the rest of this study, automatic soot alpha correction modeling was used to estimate the alpha correction factors.

Figure 4.16 illustrates the effect of adding an increasing number of soot precursor species. As more species are added to the custom precursor list, the soot yield increases in both volume fraction and soot mass yield. CONVERGE calculates the rate of soot inception rate as [66, 71]:

$$\dot{Q}_{i,pi} = 2v_{PAH}\beta_{fm,pi}(v_{PAH})N_{PAH}^2 \tag{4.2}$$

Here, v_{PAH} is the volume of the PAH species, $\beta_{fm,pi}$ is the collision coefficient and N_{PAH} is the number density of the PAH species. With a higher number of soot precursor species, more PAHs participate in the inception reaction and affect the subsequent soot formation stages increasing the overall soot yield.

From figures 4.15a and 4.15c it is apparent that the variation in settings does not negatively affect the combustion process in the simulation with the PSM model using the Kalvakala mechanism.

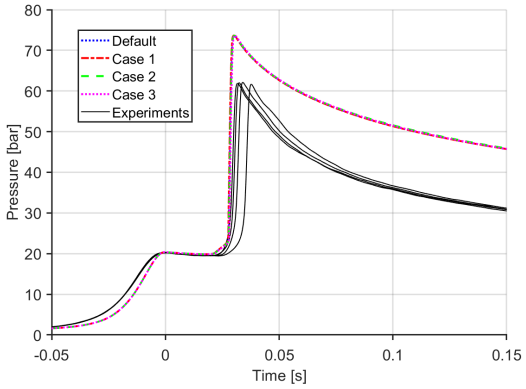

(a) Main Chamber Pressure Traces

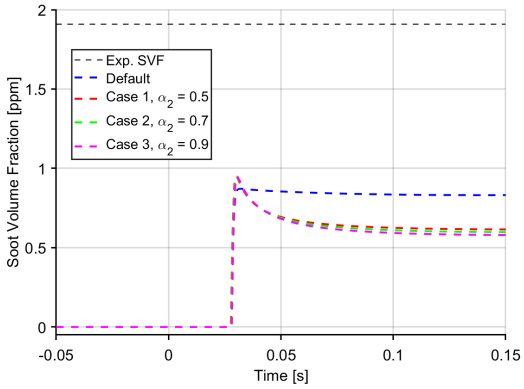

(b) Soot Volume Fraction vs Time

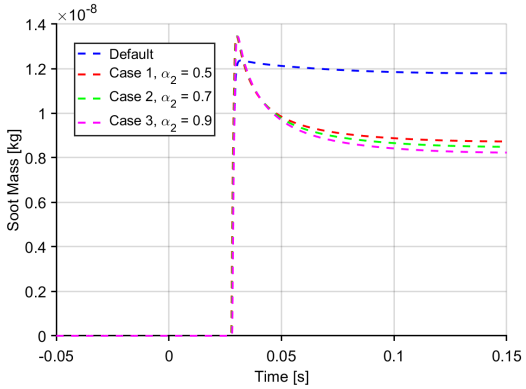

(c) Soot Mass vs Time

Figure 4.15: PSM model parameter sweep results, α correction factors

4.7 Final Model and Results

Four different gasoline-ethanol blend fuels starting from E10 (10% v/v) to E100 was tested. The CFD model was updated incorporating the improvements made throughout the project. The detailed settings of this model are illustrated in table 4.3.

The fuels were tested at various equivalence range starting from stoichiometric to richer conditions. The experiments were limited by the laser diagnostics to optically thick conditions, richer conditions where laser transmittance dropped to zero and no further meaningful data could be taken. Since the CFD is not limited by this, richer cases than the experimental optical

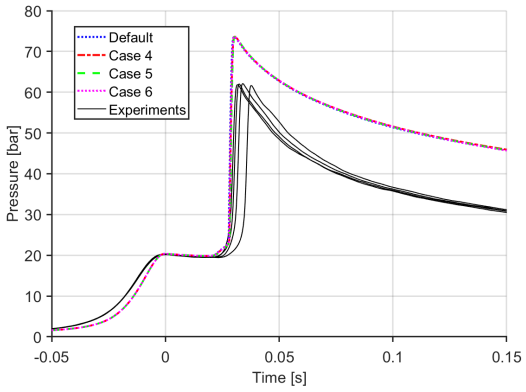

(a) Main Chamber Pressure Traces

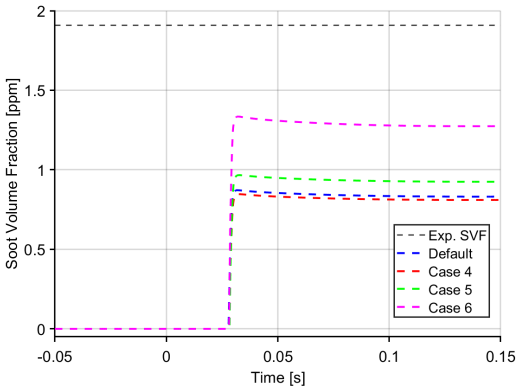

(b) Soot Volume Fraction vs Time

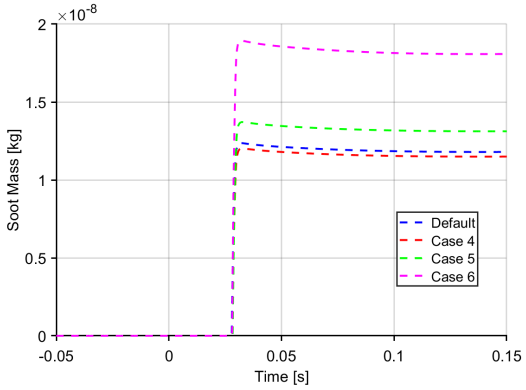

(c) Soot Mass vs Time

Figure 4.16: PSM model parameter sweep results, soot inception species

Table 4.3: Settings for Final CFD Model

Geometry	1/6th Sector
Mesh Settings	**Cell Size**
Base Grid	2.0 mm
Fixed Embedding	**Cell Size**
Head	0.5mm
Liner Main	0.5mm
Liner Crevice	0.5mm
Piston Crevice	0.25mm
Piston Top	0.5mm
Adaptive Mesh Refinement (AMR)	**Cell Size**
Velocity	0.25mm
Temperature	0.25mm
Chemical Kinetic Mechanism	Kalvalkala Mechanism
Soot Models	Hiroyasu-NSC
	Particulate Size Mimic (PSM)

Table 4.4: Test conditions for different fuels in experiment and simulation

Fuel		Eq. Ratio	$P_{comp}[bar]$	$T_{comp}[K]$
E10	**Exp**	1.0 - 2.0	20 ± 1	660 ± 10
	CFD	1.0 - 2.4	20 ± 0.6	663 ± 5
E30	**Exp**	1.0 - 2.2	20 ± 1	675 ± 10
	CFD	1.0 - 2.6	20.5 ± 0.3	682 ± 3
E85	**Exp**	1.0 - 2.66	20 ± 1	780 ± 10
	CFD	1.0 - 3.0	19.5 ± 0.3	800 ± 10
E100	**Exp**	1.0 - 2.8	20 ± 1	790 ± 10
	CFD	1.0 - 3.28	19.1 ± 0.3	810 ± 5

thick conditions were run to extend the soot formation curve. Table 4.4 details the conditions used for all the different fuels for experiments and CFD simulations. To maintain somewhat similar ignition delay times, the compressed temperatures had to be increased with the increase in ethanol content in the fuel. Another thing of note is, with increasing amount of ethanol in the fuel the rich limit in experiments were extended, showing that increasing amounts of ethanol in the fuel blend correspond with decreasing levels of soot formation.

Figure 4.17 illustrates the ignition delay times for different gasoline-ethanol blends levels compared between the CFD model and experiments. For the E10 fuel the ignition delay is quite consistently advanced for the simulation model. The ignition delay times are more closely matched for the E30 fuel. For the higher ethanol content fuels E85 and E100, the compressed temperatures in the CFD models had to be increased by about 20K at each equivalence ratios to get ignition timing somewhat close to the experiments. The surrogate fuel model had to be optimized to be used with all the different blend levels, as such the reactivity of the surrogate blend fuel differs from the real blend fuel, which become really apparent from the ignition delay plots. It can be surmised that the reactivity of the ethanol in the model is lower than the real fuel

grade ethanol, and vice-versa for the gasoline. This results in the lower ethanol content E10 fuel being more reactive (shorter ignition delay) and higher ethanol content E85 and E100 having lower reactivity (need for higher compressed temperature).

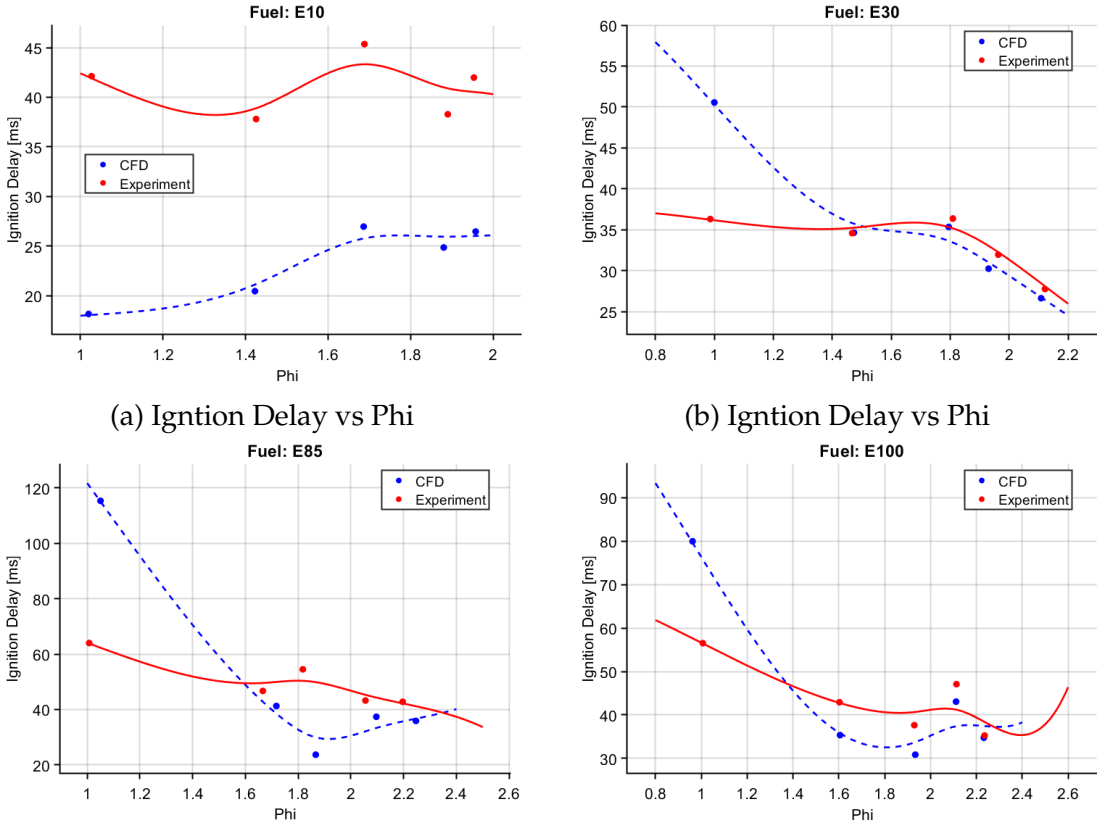

(a) Igntion Delay vs Phi

(b) Igntion Delay vs Phi

(c) Igntion Delay vs Phi

(d) Igntion Delay vs Phi

Figure 4.17: Ignition Delays For Various Gasoline-Ethanol Fuel Blends

The soot volume fraction for the different fuel blends at varying equivalence ratios are presented in Figure 4.18. Results from the two soot models, Hiroyasu-NSC and PSM, in both the default and tuned settings are illustrated. For a fair comparison to the experimental results, the soot volume fraction results from the CFD were averaged for a duration of 100ms, starting 25ms post ignition,

hence every single data point represents a equivalence ratio (phi) - soot volume fraction pairing. It should also be noted The equivalence ratio where the fuel blends start making exponentially more soot will be referred to as critical phi for the sake of coherence and brevity.

For the E10 fuel (Figure 4.18a) the default Hiyoasu model massively underpredicts the soot. The default PSM model predicts soot better, especially at lower equivalence ratios, but the critical phi where E10 starts making significantly more soot is overpredicted slightly. The tuned Hiroyasu and PSM model do a better job at predicting the critical phi condition but still significantly underpredict soot formation levels.

Figure 4.18b illustrates the results for E30 fuel and the CFD model overall performs better. The default Hiroyasu model, as expected, underperforms. The default PSM model well predicts the critical phi. The tuned Hiroyasu and tuned PSM model do a very good job at predicting the critical phi and slightly overpredicts the soot volume fraction just before the critical point. Similar to the ignition delay prediction, the surrogate fuel along with the chemical kinetic model is well balanced for the E30 fuel, which results in good prediction of the sooting characteristics as well.

With the E85 fuel (Figure 4.18c) an interesting thing to note is that the deafult and tuned PSM model have very similar soot yield. Even with the additional PAHs the soot yield has not increased significantly, further investigation in the mass production of these PAHs species in the future can provide some insight into the combustion and post-combustion chemistry of these fuels. For this fuel, the tuned Hiroyasu model does a better job at predicting soot yield and also the critical phi.

The soot yield of E100 fuel illustrated in Figure 4.18d also tells a similar story. The default Hiroyasu model, the default PSM model and the tuned PSM

model all form less soot than predicted by the experiments. They're also very similar in their soot yield upto about a equivalence ratio of about 2.25. All of these fail to capture the critical phi. In this case as with the E85 fuel, the tuned Hiroyasu model actually does a superior prediction of soot formation as well the critical phi, at least upto an equivalence ratio of about 2.1.

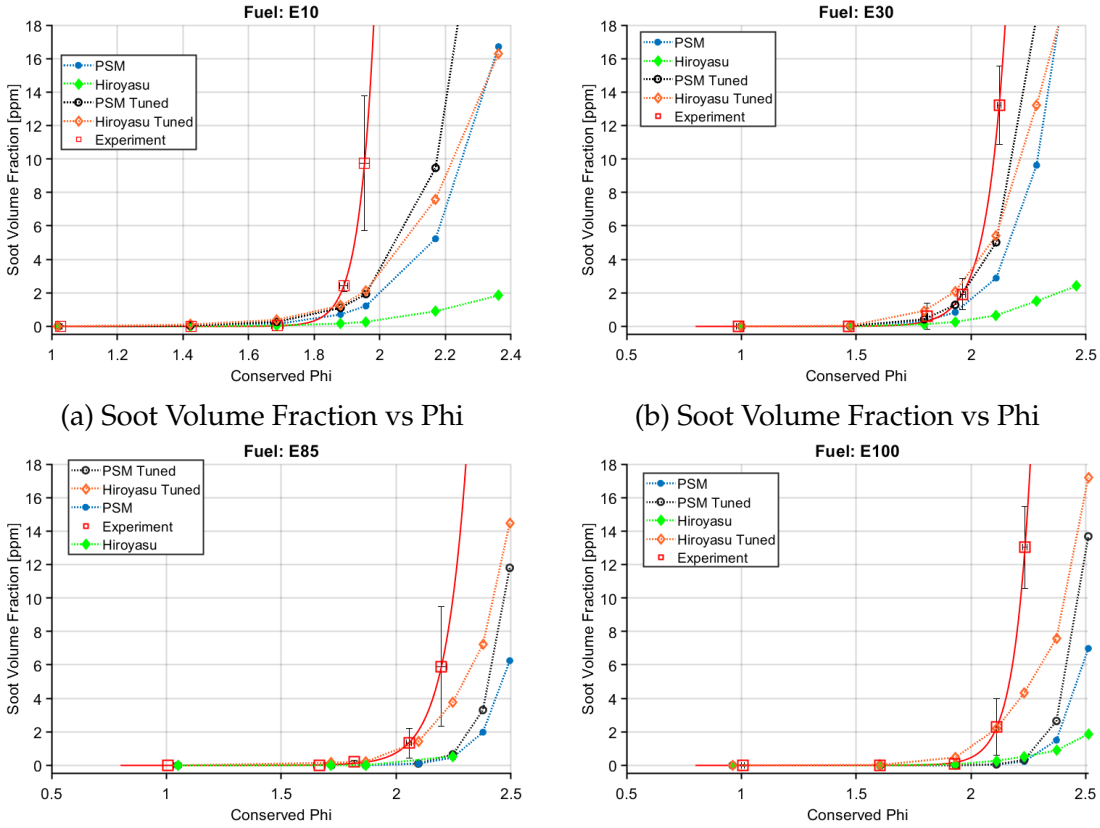

(a) Soot Volume Fraction vs Phi

(b) Soot Volume Fraction vs Phi

(c) Soot Volume Fraction vs Phi

(d) Soot Volume Fraction vs Phi

Figure 4.18: Soot Formation For Various Gasoline-Ethanol Fuel Blends

The two different soot models in their default and tuned state with the four different fuel blends illustrate the current capabilities of three dimensional CFD models in predicting soot. It's also of note from Figure 4.18 that with the increase of ethanol content in the fuel, the soot vs equivalence ratio curve

progressively shifts to the right indicating that with higher ethanol content, the fuels are less likely to soot at a specific equivalence ratio.

CHAPTER 5

FUTURE WORK

Several different soot models available in commercial CFD solver CONVERGE 3.0 along with some publicly available chemical kinetics models were evaluated for the models capabilities in predicting the sooting tendencies of gasoline-ethanol blend fuels. The model was found to be adequate at predicting the combustion characteristics of real fuel but the soot formation was underpredicted across all the fuel blends and equivalence ratios. There is still a lot of progress to be made to in modeling soot formation, especially for these lighter fuels. The soot models were tuned within their limits to improve the soot prediction capabilities. While they do improve the overall performance of the model, they still fall short of predicting the experiments accurately. The models performed well qualitatively in terms of capturing the general trend of soot formation for gasoline-ethanol blend fuels at richer conditions.

Future work will continue to investigate these soot models with different chemical kinetic models. The mechanisms themselves can be adjusted to bring the fuel reactivity of ethanol more in line with experimental results as well as to improve the fidelity in predicting the formation of PAH species. The peak pressure discrepancy between the experiments and the CFD model will also be further investigated, both numerically and experimentally. A possible upgrade to the RCM, an optical head will enable us to image the combustion process more closely and can be another source of validation of the combustion models of the CFD. It can also shed more light on the assumption of an homogeneous soot cloud formation post ignition. Further improvement to the CFD model will include methods to compute the soot volume fraction inside the cylinder with a line of sight method to make more equitable comparison to the experiments.

The natural progression of this research will also see development of engine CFD model with soot prediction capabilities and engine experiments with gasoline-ethanol blend fuels under mixing controlled combustion. This will test the capabilities of the CFD model in the complex environment inside an engine as well as further develop knowledge of the sooting tendencies of lighter fuels in heavy duty engines and advanced combustion strategies.

BIBLIOGRAPHY

[1] James E. Anderson, Thomas G. Leone, Michael H. Shelby, Timothy J. Wallington, Jeffrey J. Bizub, Michael Foster, Michael G. Lynskey, and Dusan Polovina. Octane numbers of ethanol-gasoline blends: Measurements and novel estimation method from molar composition. In *SAE Technical Papers*. SAE International, 2012. ISSN: 26883627.

[2] J. C.G. Andrae. Development of a detailed kinetic model for gasoline surrogate fuels. *Fuel*, 87(10-11):2013–2022, August 2008.

[3] J. C.G. Andrae and R. A. Head. HCCI experiments with gasoline surrogate fuels modeled by a semidetailed chemical kinetic model. *Combustion and Flame*, 156(4):842–851, April 2009.

[4] Mathieu André, Bruno Walter, Gilles Bruneaux, Fabrice Foucher, and Christine Mounaïm–Rousselle. Exhaust gas recirculation stratification to control diesel homogeneous charge compression ignition combustion. *International Journal of Engine Research*, 13(5):429–447, October 2012.

[5] Allen W. (Bill) Gray and Thomas W. Ryan. Homogeneous Charge Compression Ignition (HCCI) of Diesel Fuel. page 971676, May 1997.

[6] Daniel Blom, Maria Karlsson, Kent Ekholm, Per Tunestål, and Rolf Johansson. HCCI Engine Modeling and Control using Conservation Principles. April 2008.

[7] Nicolas Bourgeois, S. Scott Goldsborough, Hervé Jeanmart, and Francesco Contino. CFD simulations of Rapid Compression Machines using detailed chemistry: Evaluation of the 'crevice containment' concept. *Combustion and Flame*, 189:225–239, March 2018. Publisher: Elsevier Inc.

[8] L. R. Cancino, M. Fikri, A. A.M. Oliveira, and C. Schulz. Ignition delay times of ethanol-containing multi-component gasoline surrogates: Shock-tube experiments and detailed modeling. *Fuel*, 90(3):1238–1244, March 2011.

[9] Marco Chiodi, Andreas Kaechele, Michael Bargende, Donatus Wichelhaus, and Christian Poetsch. Development of an Innovative Combustion Process: Spark-Assisted Compression Ignition. *SAE International Journal of Engines*, 10(5):2486–2499, September 2017.

[10] Muhammad A. Chishty, Michele Bolla, Evatt R. Hawkes, Yuanjiang Pei, and Sanghoon Kook. Soot formation modelling for n-dodecane sprays using the

transported PDF model. *Combustion and Flame*, 192:101–119, June 2018. Publisher: Elsevier Inc.

[11] Musharrat Chowdhury and Adam Dempsey. Inverted Reactivity Controlled Compression Ignition (iRCCI) with Methanol Fuel & Reactivity Enhancers. pages 2022–01–0464, March 2022.

[12] J Clarkson, J.F Griffiths, J.P MacNamara, and B.J Whitaker. Temperature fields during the development of combustion in a rapid compression machine. *Combustion and Flame*, 125(3):1162–1175, May 2001.

[13] Scott Curran, Vitaly Prikhodko, Kukwon Cho, C. Scott Sluder, James Parks, Robert Wagner, Sage Kokjohn, and Rolf D. Reitz. In-Cylinder Fuel Blending of Gasoline/Diesel for Improved Efficiency and Lowest Possible Emissions on a Multi-Cylinder Light-Duty Diesel Engine. pages 2010–01–2206, October 2010.

[14] John E. Dec and Wontae Hwang. Characterizing the Development of Thermal Stratification in an HCCI Engine Using Planar-Imaging Thermometry. *SAE International Journal of Engines*, 2(1):421–438, April 2009.

[15] John E. Dec, Wontae Hwang, and Magnus Sjöberg. An Investigation of Thermal Stratification in HCCI Engines Using Chemiluminescence Imaging. pages 2006–01–1518, April 2006.

[16] Adam Dempsey, Musharrat Chowdhury, Sage Kokjohn, and Jared Zeman. Prechamber Enabled Mixing Controlled Combustion - A Fuel Agnostic Technology for Future Low Carbon Heavy-Duty Engines. pages 2022–01–0449, March 2022.

[17] Adam B. Dempsey, Scott Curran, and Rolf D. Reitz. Characterization of Reactivity Controlled Compression Ignition (RCCI) Using Premixed Gasoline and Direct-Injected Gasoline with a Cetane Improver on a Multi-Cylinder Engine. *SAE International Journal of Engines*, 8(2):859–877, April 2015.

[18] Adam B Dempsey, Scott J Curran, and Robert M Wagner. A perspective on the range of gasoline compression ignition combustion strategies for high engine efficiency and low NOx and soot emissions: Effects of in-cylinder fuel stratification. *International Journal of Engine Research*, 17(8):897–917, October 2016.

[19] Adam B. Dempsey, Patrick Seiler, Kenth Svensson, and Yongli Qi. A Comprehensive Evaluation of Diesel Engine CFD Modeling Predictions

Using a Semi-Empirical Soot Model over a Broad Range of Combustion Systems. *SAE International Journal of Engines*, 11(6):2018–01–0242, April 2018.

[20] Adam B. Dempsey, N. Ryan Walker, and Rolf D. Reitz. Effect of Cetane Improvers on Gasoline, Ethanol, and Methanol Reactivity and the Implications for RCCI Combustion. *SAE International Journal of Fuels and Lubricants*, 6(1):170–187, April 2013.

[21] Brian Gainey, James Gohn, Ziming Yan, Khurram Malik, Mozhgan Rahimi Boldaji, and Benjamin Lawler. HCCI with Wet Ethanol: Investigating the Charge Cooling Effect of a High Latent Heat of Vaporization Fuel in LTC. pages 2019–24–0024, September 2019.

[22] Brian Gainey, Ziming Yan, James Gohn, Mozhgan Rahimi Boldaji, and Benjamin Lawler. TSCI with Wet Ethanol: An Investigation of the Effects of Injection Strategy on a Diesel Engine Architecture. pages 2019–01–1146, April 2019.

[23] Brian Gainey, Ziming Yan, Mozhgan Rahimi-Boldaji, and Benjamin Lawler. On the Effects of Injection Strategy, EGR, and Intake Boost on TSCI With Wet Ethanol. In *ASME 2019 Internal Combustion Engine Division Fall Technical Conference*, page V001T03A006, Chicago, Illinois, USA, October 2019. American Society of Mechanical Engineers.

[24] Gerald Gentz, Bryce Thelen, Paul Litke, John Hoke, and Elisa Toulson. Combustion Visualization, Performance, and CFD Modeling of a Pre-Chamber Turbulent Jet Ignition System in a Rapid Compression Machine. *Source: SAE International Journal of Engines*, 8(2):538–546, 2015.

[25] Masumeh Gholamisheeri, Bryce Thelen, Gerald Gentz, and Elisa Toulson. CFD Modeling of an Auxiliary Fueled Turbulent Jet Ignition System in a Rapid Compression Machine. In *SAE Technical Papers*, volume 2016-April. SAE International, April 2016. Issue: April ISSN: 01487191.

[26] Masumeh Gholamisheeri, Bryce Thelen, and Elisa Toulson. CFD Modeling and Experimental Analysis of a Homogeneously Charged Turbulent Jet Ignition System in a Rapid Compression Machine. In *SAE Technical Papers*, volume 2017-March. SAE International, March 2017. Issue: March ISSN: 01487191.

[27] S S Goldsborough, S Hochgreb, G Vanhove, M S Wooldridge, H J Curran, and C.-J Sung. Advances in rapid compression machine studies of low-and intermediate-temperature autoignition phenomena. Technical report, 2017.

[28] S. S. Goldsborough, G. Mittal, and C. Banyon. Methodology to account for multi-stage ignition phenomena during simulations of RCM experiments. *Proceedings of the Combustion Institute*, 34(1):685–693, 2013. Publisher: Elsevier Ltd.

[29] S. Scott Goldsborough, Colin Banyon, and Gaurav Mittal. A computationally efficient, physics-based model for simulating heat loss during compression and the delay period in RCM experiments. *Combustion and Flame*, 159(12):3476–3492, December 2012.

[30] Philippe Guibert, Alan Keromnes, and Guillaume Legros. An Experimental Investigation of the Turbulence Effect on the Combustion Propagation in a Rapid Compression Machine. *Flow, Turbulence and Combustion*, 84(1):79–95, January 2010.

[31] John B. Heywood. *Internal Combustion Engine Fundamentals*. McGraw-Hill, 1988.

[32] H. Hiroyasu and T. Kadota. Models for Combustion and Formation of Nitric Oxide and Soot in Direct Injection Diesel Engines. page 760129, February 1976.

[33] Kazuhisa Inagaki, Takayuki Fuyuto, Kazuaki Nishikawa, Kiyomi Nakakita, and Ichiro Sakata. Dual-Fuel PCI Combustion Controlled by In-Cylinder Stratification of Ignitability. pages 2006–01–0028, April 2006.

[34] Intergovernmental Panel on Climate Change. Working Group III and Ottmar Edenhofer. *Climate change 2014 : mitigation of climate change : Working Group III contribution to the Fifth Assessment Report of the Intergovernmental Panel on Climate Change*.

[35] Dongwon Jung. Autoignition and Chemical-Kinetic Mechanisms of Homogeneous Charge Compression Ignition Combustion for the Fuels with Various Autoignition Reactivity. In Muhammad Akhyar Farrukh, editor, *Advanced Chemical Kinetics*. InTech, February 2018.

[36] John Kaddatz, Michael Andrie, Rolf D. Reitz, and Sage Kokjohn. Light-Duty Reactivity Controlled Compression Ignition Combustion Using a Cetane Improver. April 2012.

[37] Krishna C. Kalvakala, Pinaki Pal, Jorge Pulpeiro Gonzalez, Christopher P. Kolodziej, Hee Je Seong, Goutham Kukkadapu, Matthew McNenly, Scott Wagnon, Russell Whitesides, Nils Hansen, and Suresh K. Aggarwal. Numerical analysis of soot emissions from gasoline-ethanol and

gasoline-butanol blends under gasoline compression ignition conditions. *Fuel*, 319, July 2022. Publisher: Elsevier Ltd.

[38] John Kempf, Adam Dempsey, and Casey Allen. Autoignition and Sooting Characteristics of *Iso* -Octane and Ethanol in an Optical Rapid Compression Machine. pages 2022–01–0419, March 2022.

[39] Richard Kempf. Autoignition and Sooting Characteristics of Iso-Octane and Ethanol in an Optical Rapid Compression Machine. *Master's Theses (2009 -)*, July 2022.

[40] Nick J. Killingsworth, Tuan M. Nguyen, Carter Brown, Goutham Kukkadapu, and Julien Manin. Investigating the Effects of Chemical Mechanism on Soot Formation Under High-Pressure Fuel Pyrolysis. *Frontiers in Mechanical Engineering*, 7:765478, November 2021.

[41] T Kitamura, T Ito, J Senda, and H Fujimoto. Mechanism of smokeless diesel combustion with oxygenated fuels based on the dependence of the equivalence ration and temperature on soot particle formation. *International Journal of Engine Research*, 3(4):223–248, August 2002.

[42] S L Kokjohn, R M Hanson, D A Splitter, and R D Reitz. Fuel reactivity controlled compression ignition (RCCI): a pathway to controlled high-efficiency clean combustion. *International Journal of Engine Research*, 12(3):209–226, June 2011.

[43] Sage L. Kokjohn, Reed M. Hanson, Derek A. Splitter, and Rolf D. Reitz. Experiments and Modeling of Dual-Fuel HCCI and PCCI Combustion Using In-Cylinder Fuel Blending. *SAE International Journal of Engines*, 2(2):24–39, November 2009.

[44] Sage L Kokjohn and Rolf D Reitz. Reactivity controlled compression ignition and conventional diesel combustion: A comparison of methods to meet light-duty NOx and fuel economy targets. *International Journal of Engine Research*, 14(5):452–468, October 2013.

[45] Song-Charng Kong, Yong Sun, and Rolf D. Reitz. Modeling Diesel Spray Flame Lift-Off, Sooting Tendency and NOx Emissions Using Detailed Chemistry With Phenomenological Soot Model. In *ASME 2005 Internal Combustion Engine Division Spring Technical Conference*, pages 149–157. ASMEDC, January 2005.

[46] Sanjeev Kumar and D. Ramkrishna. On the solution of population balance equations by discretization—II. A moving pivot technique. *Chemical*

Engineering Science, 51(8):1333–1342, April 1996.

[47] Benjamin Lawler, Derek Splitter, James Szybist, and Brian Kaul. Thermally Stratified Compression Ignition: A new advanced low temperature combustion mode with load flexibility. *Applied Energy*, 189:122–132, March 2017.

[48] Uisung Lee, Hoyoung Kwon, May Wu, and Michael Wang. Retrospective analysis of the U.S. corn ethanol industry for 2005 – 2019: implications for greenhouse gas emission reductions. *Biofuels, Bioproducts and Biorefining*, 15(5):1318–1331, September 2021.

[49] Yaopeng Li, Ming Jia, Leilei Xu, and Xue-Song Bai. Multiple-objective optimization of methanol/diesel dual-fuel engine at low loads: A comparison of reactivity controlled compression ignition (RCCI) and direct dual fuel stratification (DDFS) strategies. *Fuel*, 262:116673, February 2020.

[50] Xinlei Liu, Hu Wang, Zunqing Zheng, Jialin Liu, Rolf D. Reitz, and Mingfa Yao. Development of a combined reduced primary reference fuel-alcohols (methanol/ethanol/propanols/butanols/n-pentanol) mechanism for engine applications. *Energy*, 114:542–558, November 2016. Publisher: Elsevier Ltd.

[51] Caroline Marchal. *Modélisation de la formation et de l'oxydation des suies dans un moteur automobile*. Theses, Université d'Orléans, December 2008.

[52] Fabian Mauß. *Entwicklung eines kinetischen Modells der Rußbildung mit schneller Polymerisation*. Cuvillier, Göttingen, 1. aufl edition, 1998.

[53] M.V. Maylin, M.V. Kirgina, E.V. Sviridova, B.V. Sakhnevitch, and E.D. Ivanchina. Calculation of Gasoline Octane Numbers Taking into Account the Reaction Interaction of Blend Components. *Procedia Chemistry*, 10:477–484, 2014. Publisher: Elsevier BV.

[54] Gisele Mendes, Helga G. Aleme, and Paulo J.S. Barbeira. Determination of octane numbers in gasoline by distillation curves and partial least squares regression. *Fuel*, 97:131–136, July 2012.

[55] Gaurav Mittal, Mandhapati P. Raju, and Chih Jen Sung. Computational fluid dynamics modeling of hydrogen ignition in a rapid compression machine. *Combustion and Flame*, 155(3):417–428, November 2008.

[56] Gaurav Mittal, Mandhapati P. Raju, and Chih Jen Sung. CFD modeling of two-stage ignition in a rapid compression machine: Assessment of

zero-dimensional approach. *Combustion and Flame*, 157(7):1316–1324, July 2010.

[57] Gaurav Mittal and Chih-Jen Sung. Aerodynamics inside a rapid compression machine. *Combustion and Flame*, 145(1-2):160–180, April 2006.

[58] Charles J. Mueller and Mark P. Musculus. Glow Plug Assisted Ignition and Combustion of Methanol in an Optical DI Diesel Engine. pages 2001–01–2004, May 2001.

[59] Mark E. Myers, Janis. Stollsteimer, and Andrew M. Wims. Determination of gasoline octane numbers from chemical composition. *Analytical Chemistry*, 47(13):2301–2304, November 1975.

[60] J. NAGLE and R.F. STRICKLAND-CONSTABLE. OXIDATION OF CARBON BETWEEN 1000–2000°C. *Proceedings of the Fifth Conference on Carbon*, pages 154–164, 1962.

[61] Paul M. Najt and David E. Foster. Compression-Ignited Homogeneous Charge Combustion. February 1983.

[62] Karl Netzell. *Development and Applications of Detailed Kinetic Models for the Soot Particle Size Distribution Function*. thesis/doccomp, Lund University, 2006.

[63] John Neuman. Development of a Rapid Compression Controlled-Expansion Machine for Chemical Ignition Studies. Technical report, 2009.

[64] Mozhgan Rahimi Boldaji, Brian Gainey, and Benjamin Lawler. Thermally stratified compression ignition enabled by wet ethanol with a split injection strategy: A CFD simulation study. *Applied Energy*, 235:813–826, February 2019.

[65] Shuojin Ren, Sage L. Kokjohn, Zhi Wang, Haoye Liu, Buyu Wang, and Jianxin Wang. A multi-component wide distillation fuel (covering gasoline, jet fuel and diesel fuel) mechanism for combustion and PAH prediction. *Fuel*, 208:447–468, November 2017.

[66] K. J Richards, P. K. Senecal, and E. Pomraning. CONVERGE 3.0 Manual, 2021.

[67] Dennis Robertson and Robert Prucka. A Review of Spark-Assisted Compression Ignition (SACI) Research in the Context of Realizing Production Control Strategies. pages 2019–24–0027, September 2019.

[68] P. K. Senecal, E. Pomraning, K. J. Richards, T. E. Briggs, C. Y. Choi, R. M. Mcdavid, and M. A. Patterson. Multi-Dimensional Modeling of Direct-Injection Diesel Spray Liquid Length and Flame Lift-off Length using CFD and Parallel Detailed Chemistry. March 2003.

[69] Magnus Sjöberg and John E. Dec. Smoothing HCCI Heat-Release Rates Using Partial Fuel Stratification with Two-Stage Ignition Fuels. pages 2006–01–0629, April 2006.

[70] Magnus Sjöberg, John E. Dec, and Nicholas P. Cernansky. Potential of Thermal Stratification and Combustion Retard for Reducing Pressure-Rise Rates in HCCI Engines, Based on Multi-Zone Modeling and Experiments. pages 2005–01–0113, April 2005.

[71] Marian von Smoluchowski. Versuch einer mathematischen Theorie der Koagulationskinetik kolloider Lösungen. *Zeitschrift fuer physikalische Chemie <Leipzig>*, 92:129 – 168, 2010.

[72] Chih Jen Sung and Henry J. Curran. Using rapid compression machines for chemical kinetics studies. *Progress in Energy and Combustion Science*, 44:1–18, 2014. Publisher: Elsevier Ltd.

[73] James P. Szybist. Fuel-Specific Effect of Exhaust Gas Residuals on HCCI Combustion: A Modeling Study. pages 2008–01–2402, October 2008.

[74] Dale R. Tree and Kenth I. Svensson. Soot processes in compression ignition engines. *Progress in Energy and Combustion Science*, 33(3):272–309, June 2007.

[75] OAR US EPA. Global Greenhouse Gas Emissions Data, January 2016.

[76] Chaitanya Wadkar and Elisa Toulson. CFD study of the effect of initial temperature inhomogeneities and buoyancy on the autoignition behavior of ethanol in an RCM. *Energy and Fuels*, 35(21):17876–17889, November 2021. Publisher: American Chemical Society.

[77] S Walton, X He, B Zigler, M Wooldridge, and A Atreya. An experimental investigation of iso-octane ignition phenomena. *Combustion and Flame*, 150(3):246–262, August 2007.

[78] John Z. Wen, M.J. Thomson, S.H. Park, S.N. Rogak, and M.F. Lightstone. Study of soot growth in a plug flow reactor using a moving sectional model. *Proceedings of the Combustion Institute*, 30(1):1477–1484, January 2005.

[79] David Wilson. Application of a Multi-Zone Model for the Prediction of Species Concentrations in Rapid Compression Machine Experiments. Technical report.

[80] J. Würmel and J. M. Simmie. CFD studies of a twin-piston rapid compression machine. *Combustion and Flame*, 141(4):417–430, June 2005.

[81] Yuchen Ya, Xiaokang Nie, Licheng Peng, Longkai Xiang, Jialong Hu, Wenlong Dong, and Huaqiang Chu. Effects of Ethanol Blending on the Formation of Soot in n-Heptane/Air Coflow Diffusion Flame. *Journal of Chemistry*, 2020, 2020. Publisher: Hindawi Limited.

[82] Linjun Yu, Yanfei Li, Bowen Li, Hao-ye Liu, Zhi Wang, Xin He, and Shi-jin Shuai. Comparative Study on Gasoline HCCI and DICI Combustion in High Load Range with High Compression Ratio for Passenger Cars Application. *SAE International Journal of Fuels and Lubricants*, 10(3):2017–01–2257, October 2017.

[83] Yan Zhang, Bang-Quan He, Hui Xie, and Hua Zhao. The Combustion and Emission Characteristics of Ethanol on a Port Fuel Injection HCCI Engine. pages 2006–01–0631, April 2006.

[84] Bei Jing Zhong and Dong Zheng. A chemical mechanism for ignition and oxidation of multi-component gasoline surrogate fuels. *Fuel*, 128:458–466, July 2014. Publisher: Elsevier Ltd.

[85] Tianyuan Zhou, Changsheng Yao, Fuyuan Yang, and Sun Jinwei. Glow Plug Assisted Compression Ignition (GA-CI) in Cold Conditions. pages 2017–01–2288, October 2017.